Bulk and interfacial wetting properties of binary liquid mixtures

T. Getta and S. Dietrich

Fachbereich Physik, Bergische Universität Wuppertal, Postfach 100127, D-5600 Wuppertal 1, Germany

(Received 12 October 1992)

We classify the interfacial wetting behavior of binary liquid mixtures at their liquid-vapor interface. The criteria with respect to the atomic interactions between the two species are whether the Hamaker constant of that interface fulfills either sufficient conditions for the absence of a wetting transition, or the necessary conditions for critical wetting, or the necessary conditions either for being wet already at low temperatures or for undergoing a first-order wetting transition upon approaching the critical end point along the triple line. Based on the Blume-Emery-Griffiths model and on the Percus-Yevick theory we scan the parameter space that determines the structure of the bulk phase diagrams. By analyzing the absolute values of the Hamaker constant we pay particular attention to interfacial wetting induced by tricritical points. In addition, we compare the predictions of the Percus-Yevick theory for the bulk phase diagrams and the number densities of the fluid bulk phases with experimental and simulation data as well as with different theoretical approaches.

I. INTRODUCTION

Binary liquid mixtures consisting of two sorts of molecules, called A and B, give rise to a rich variety of wetting phenomena. In general, a wetting transition describes the formation of a thermodynamic stable layer of a third phase at an interface between two other phases. If at a wetting transition the thickness of the wetting layer grows continuously to infinity, it is called *critical wetting*, whereas in the case of a discontinuous jump to infinity it is called *first-order wetting*. A detailed discussion of various wetting phenomena is given in Ref. [1], for earlier reviews see Refs. [2–7]. An excellent introduction to this subject is given in Ref. [8]. The general features of wetting phenomena of binary liquid mixtures at a wall have been discussed in Ref. [9]. Recent experiments for wetting of a wall by binary liquid mixtures have been performed by Pohl and Goldburg [10], Beysens and Estéve [11], Sigl and Fenzl [12], and by Franck and co-workers [13–16].

Both in theory and experiment, the presence of a wall complicates a precise determination of the interfacial structures. The wetting phenomena depend not only on the atomic interactions between the components of the binary liquid mixtures, but also on two substrate potentials acting on the A and B particles, respectively. In addition, close to the wall the substrate potentials lead to density oscillations (see Sec. III B in Ref. [1]), which signal the formation of a few solidlike layers at the wall. Third, in general the wall-liquid interface represents a nonequilibrium situation because the substrate atoms tend to dissolve in the liquid.

Binary liquid mixtures offer the opportunity to study wetting phenomena which involve fluid phases only, i.e., both coexisting bulk phases, which form the interface to be wetted, and the wetting phase itself are fluids. The *intrinsic* interface, where the wetting layer is formed, gives rise to the notation of *interfacial wetting* and represents a thermodynamically stable configuration of its own.

Due to the interfacial wetting transition the interface splits into two different interfaces, which both exhibit capillary waves. Since fluid mixtures are governed by long-range van der Waals forces, the leading singularities of continuous wetting transitions are unaffected by capillary waves. This allows us to treat these interfacial wetting phenomena within mean-field theory (MFT) (see Ref. [17] and Sec. IV C in Ref. [1]).

Interfacial wetting depends only on those interactions, which determine simultaneously the bulk properties of binary liquid mixtures, i.e., the interactions among the A particles and among the B particles themselves and on the interaction between the A and B particles. Therefore certain features of interfacial wetting phenomena are fixed by *bulk* properties of the participating phases.

There is practically an unlimited number of different binary liquid mixtures accessible to experiments. Numerous experimental studies of interfacial wetting [18–31] have explored only a very small subset of possible binary liquid mixtures. As in the case of experiments, only for a few particular binary mixtures interfacial wetting has been studied theoretically by taking into account the long-range character of the interactions for equal radii [32–34]. In order to provide some guidance for further exploration we classify the possible interfacial wetting behavior of binary liquid mixtures on the basis of their bulk properties by taking into account the influence of different atomic radii.

Following Scott and van Konynenburg [35] the variety of binary liquid mixtures is systematically classified by the different structures of their phase diagrams. Figure 1 shows the three different phase diagrams of type II and III accessible to our investigations. At low temperatures both type-II and -III phase diagrams contain three different phases, an A-rich liquid phase in which the number density ρ_A of A particles is larger than the number density ρ_B of B particles, a B-rich liquid phase with
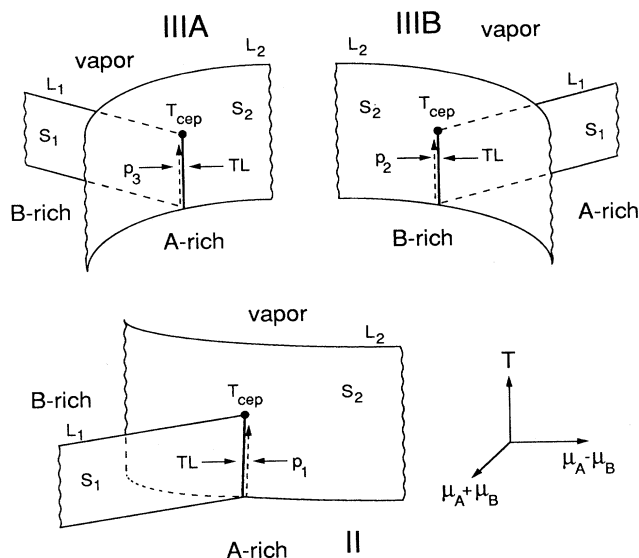
1856

FIG. 1. Type-II, -IIIA, and -IIIB bulk phase diagrams of binary liquid mixtures in the space of temperature T and the chemical potentials μ_A and μ_B. The vapor phase and the A-rich and B-rich liquid phases are separated by sheets S_1 and S_2 of first-order phase transitions. L_1 and L_2 represent lines of second-order phase transitions, TL is the triple line, which ends at the critical end point T_{cep}. The path p_1 runs on the A-rich liquid-vapor coexistence sheet along TL, p_2 runs on the B-rich liquid-vapor coexistence sheet along TL, whereas p_3 runs on the A-rich liquid–B-rich liquid coexistence sheet along TL. For reasons of clarity only one out of the three possible paths is drawn in each phase diagram and the paths are taken slightly off TL.

FIG. 2. Schematic bulk phase diagram with a tricritical point T_{tric}. We use the same notation as in Fig. 1. Three lines L_1, L_2, and L_3 of second-order phase transitions meet at the tricritical point T_{tric}.

$\rho_B > \rho_A$, and a homogeneous vapor phase. The three phases are in coexistence at the triple line, TL, and separated by the sheets S_1 and S_2 of first-order phase transitions. Upon increasing the temperature T two phases become identical at the critical line L_1 depending on the type of the phase diagram (see Fig. 1). The critical line ends at the triple line, TL, forming the critical end point T_{cep}. At higher temperatures the differences between the remaining two phases vanish at a second critical line L_2 leading to a single fluid phase.

The phase diagrams are determined by the A-A, B-B, and A-B particle interactions. By variation of the interaction parameters we are able to calculate the three different types of phase diagrams. If one changes the interaction parameters from those of type-II phase diagrams to type-III phase diagrams or from type IIIA to type IIIB a special case occurs. The critical end point touches the second critical line and becomes a tricritical point (see Fig. 2). A tricritical point (see Refs. [36] and [37]) is a point at which three different phases become identical (see Fig. 2).

All aforementioned studies of binary liquid mixtures deal with systems of type II. In Ref. [38] interfacial wetting in binary liquid mixtures with phase diagrams of type II has been analyzed and classified. This study revealed a variety of interfacial wetting phenomena. How-
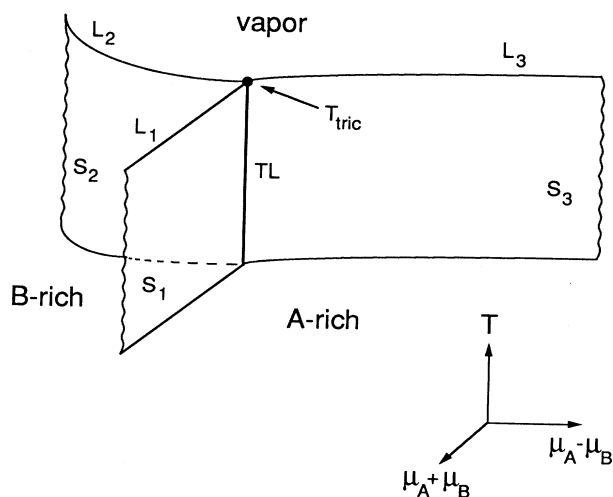
ever, numerous binary liquid mixtures are of type III, especially the rare gases, which are most suitable to theoretical approaches. Here we extend the global survey of the possible interfacial wetting behavior to binary liquid mixtures with phase diagrams of type III. Second, we calculate *absolute* values of the Hamaker constants [39], which determine the different types of interfacial wetting transitions. Third, we analyze the influence of tricritical points in the bulk on the corresponding interfacial wetting behavior.

In the first step we classify the interfacial wetting transitions for those binary liquid mixtures, which consist of particles with equal size, within the Blume-Emery-Griffiths (BEG) model (see Appendix A). Although the BEG model does not represent a quantitatively reliable description of binary liquid mixtures, it nonetheless exhibits all expected features. This eases our corresponding discussion of the Percus-Yevick (PY) theory (see Appendix B), which is a more realistic and quantitatively reliable model. The PY theory offers the opportunity to check our quantitative predictions for the bulk phase diagrams and the number densities of the fluid bulk phases with experimental and simulation data as well as with different theoretical approaches.

II. INTERFACIAL WETTING PHENOMENA IN TERMS OF THE EFFECTIVE INTERFACE POTENTIAL

A. Three thermodynamic paths

First- and second-order interfacial wetting transitions require three-phase coexistence. This condition is fulfilled on the triple line of the bulk phase diagrams of type II and III (see Fig. 1). For both types the critical end point T_{cep} can be reached along three possible thermodynamic paths.

(1) Path p_1: The A-rich liquid phase and the vapor phase are in coexistence. The wetting phase, i.e., the B-rich liquid phase, is taken to be slightly off coexistence.

(2) Path p_2: The B-rich liquid phase and the vapor phase are in coexistence. The A-rich liquid phase is the wetting phase.

(3) Path p_3: The A- and B-rich liquid phase are in coexistence so that the vapor phase is the wetting phase. This is particularly interesting for phase diagrams of type III because in this case the difference in number densities between the vapor phase and one of the liquid phases vanishes.

Figure 3 schematically shows the structure of the system along the different paths in a grand canonical ensemble without gravity. We use the notation that the α phase is in coexistence with the γ phase and that the β phase wets the α-γ interface. The peculiarities of a canonical ensemble and the effect of gravity on these structures is discussed in detail in Ref. [38].

B. Effective interface potential

Spatially inhomogeneous binary liquid mixtures and their wetting transitions are described successfully by the following density functional of the grand canonical free energy for a given configuration of the number densities $\rho_i(\mathbf{r})$ with $i = A$ and B:
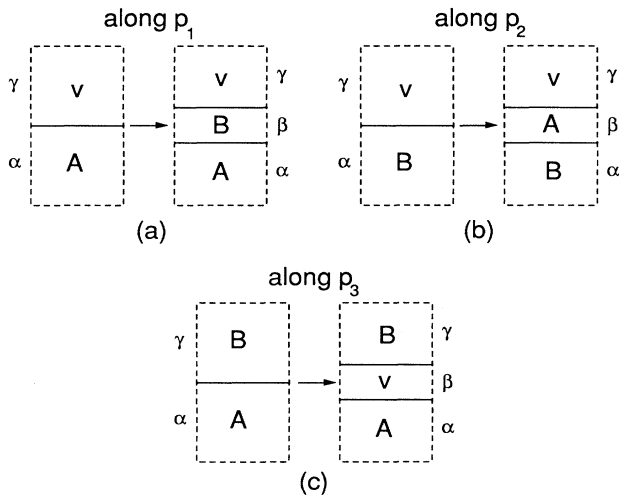
FIG. 3. (a) Interfacial wetting of the vapor–A-rich liquid interface by the B-rich liquid along the path p_1 described in Fig. 1. (b) Interfacial wetting of the vapor–B-rich liquid interface by the A-rich liquid along p_2 (see Fig. 1). (c) Interfacial wetting of the A-rich liquid–B-rich liquid interface by the vapor phase v along p_3 (see Fig. 1). The dashed lines indicate that, as in a grand canonical system, these systems are connected to a reservoir of A and B particles. The wetted phases are denoted by α and γ, and the wetting phase is called β. Along the path p_1 the α phase is A rich, the β phase is B rich, and the γ phase is the vapor phase; along the path p_2 the α phase is B rich, the β phase is A rich, and the γ phase is the vapor phase, whereas along the path p_3 the α phase is A rich, the β phase is the vapor phase, and the γ phase is B rich.

$$\Omega[\rho_i(\mathbf{r}); T, \mu_i] = \int d^3r\, f_h(\rho_i(\mathbf{r}), T)$$
$$+ \frac{1}{2} \sum_{i,j} \int d^3r \int d^3r'\, \tilde{w}_{ij}(|\mathbf{r} - \mathbf{r}'|)\rho_i(\mathbf{r})\rho_j(\mathbf{r}')$$
$$- \sum_i \mu_i \int d^3r \rho_i(\mathbf{r}) . \tag{2.1}$$

Its derivation and its status are discussed in detail in Ref. [38]. The equilibrium densities $\rho_{0,i}(\mathbf{r}; T, \mu_i)$ minimize Ω and they yield the grand canonical potential $\Omega_0(T, V, \mu_i)$. T is the temperature and V is the volume of the system, whereas μ_A and μ_B are the chemical potentials of the two species. $f_h(\rho_i(\mathbf{r}), T)$ is a suitably chosen Helmholtz free-energy density (see Appendices A and B in Ref. [38]). In this section its specific form does not matter. $\tilde{w}_{AA}$, $\tilde{w}_{BB}$, and $\tilde{w}_{AB}$ are determined by the pair potentials w_{AA}, w_{BB}, and w_{AB} [see Eq. (A26) and Appendix B of Ref. [38]]. We impose boundary conditions such that, for $z \to \pm\infty$, $\rho_{0,i}(z)$ approach the bulk values of the pure phase, depending on whether we consider path p_1, p_2, or p_3 (see Fig. 1). z denotes the direction orthogonal to the interface of area A.

For such density configurations the free-energy functional in Eq. (2.1) splits into a bulk contribution and into a surface contribution:

$$\Omega[\rho_i(\mathbf{r}); T, \mu_i] = V\Omega_b(T, \mu_i) + A\,\Omega_s[\rho_i(\mathbf{r}); T, \mu_i] . \tag{2.2}$$

At α-γ coexistence we have

$$\Omega_b(T, \mu_i) = \Omega(\rho_{i,\alpha}; T, \mu_i)/V = \Omega(\rho_{i,\gamma}; T, \mu_i)/V , \tag{2.3}$$

where $\rho_{i,\alpha}$ and $\rho_{i,\gamma}$ are the equilibrium bulk densities in the α and γ phase, respectively. From Eq. (2.1) the bulk free-energy density follows to be

$$\Omega(\rho_{i,v}; T, \mu_i)/V = f_h(\rho_{i,v}; T) - \frac{1}{2}\sum_{i,j}\hat{w}_{ij}\rho_{i,v}\rho_{j,v}$$
$$- \sum_i \mu_i \rho_{i,v} \equiv \Omega_v \tag{2.4}$$

with $v = \alpha, \beta, \gamma$ and $\Omega_\alpha = \Omega_\gamma = \Omega_b$. In Eq. (2.4) we have introduced the total strength of the (modified) interaction potentials $\hat{w}_{ij}$:

$$\hat{w}_{ij} = - \int_{\mathbb{R}^3} d^3r\, \tilde{w}_{ij}(\mathbf{r}) > 0 . \tag{2.5}$$

The surface contribution Ω_s from Eq. (2.2) gives, at its minimum, the surface tension between the α and γ phase:

$$\sigma_{\alpha,\gamma}(T, \mu_i) = \min_{\rho_i(\mathbf{r})} \Omega_s[\rho_i(\mathbf{r}); T, \mu_i]$$
$$= \min_l \Omega_s(l, T, \mu_i) = \Omega_s(l_0, T, \mu_i) . \tag{2.6}$$

$\Omega_s(l, T, \mu_i)$ is the *effective interface potential*, which is the surface free energy per area under the restriction that at the α-γ interface a wetting film with thickness l of the β-like phase is formed (see Refs. [1,40]). $\Omega_s(l, T, \mu_i)$ has the form

$$\Omega_s(l,T,\mu_i)=l(\Omega_\beta-\Omega_\gamma)+\sigma_{\alpha,\beta}+\sigma_{\beta,\gamma}+\omega(l) \qquad (2.7)$$

and is minimized by the equilibrium thickness $l_0(T,\mu_i)$. The interfacial wetting behavior depends on $\omega(l)$, which is the correction to the surface free energy due to the finite thickness of l. For large l one finds in the presence of long-range interactions [1,9,40–42]

$$\omega(l)=al^{-2}+bl^{-3}+\cdots . \qquad (2.8)$$

The leading coefficient a, which is known as Hamaker constant [39], depends only on the temperature, because for a given temperature the chemical potentials are fixed by the condition to be on the triple line. In order to evaluate the Hamaker constant we resort to its expression derived in Ref. [9]:

$$a(T)=(M_\alpha-M_\beta)(M_\beta-M_\gamma)a_j+(Q_\alpha-Q_\beta)(Q_\beta-Q_\gamma)a_K+[(Q_\alpha-Q_\beta)(M_\beta-M_\gamma)+(M_\alpha-M_\beta)(Q_\beta-Q_\gamma)]a_C , \qquad (2.9)$$

where

$$M_v=\rho_{v,A}-\rho_{v,B} , \qquad (2.10)$$

$$Q_v=\rho_{v,A}+\rho_{v,B} \qquad (2.11)$$

are linear combinations of the bulk number densities of the phase $v=\alpha,\beta,\gamma$ and

$$a_J=(t_{3,AA}-2t_{3,AB}+t_{3,BB})/8 , \qquad (2.12)$$

$$a_K=(t_{3,AA}+2t_{3,AB}+t_{3,BB})/8 , \qquad (2.13)$$

$$a_C=(t_{3,AA}-t_{3,BB})/8 . \qquad (2.14)$$

$t_{3,ij}$ are the leading coefficients in the expansion of the partly integrated interaction potentials $\tilde{w}_{ij}$:

$$t_{ij}(z)=\int_z^\infty dz'\int d^2r\,\tilde{w}_{ij}[(r^2+z'^2)^{1/2}]$$
$$=-(t_{3,ij}z^{-3}+t_{4,ij}z^{-4}+\cdots) . \qquad (2.15)$$

$a(T)$ vanishes in the limit $T\to T_{cep}$. The ratio of $a(T)$ and k_BT_{cep} is dimensionless. Upon approaching T_{cep} the Hamaker constant vanishes:

$$\frac{a(T)}{k_BT_{cep}}=\kappa\tau^\beta \quad \text{for } T\to T_{cep} \qquad (2.16)$$

with $\tau=(T_{cep}-T)/T_{cep}$ and the critical exponent $\beta=\frac{1}{2}$ (see Appendix C). The temperature dependence of $a(T)$ allows us to draw the following conclusions (see Ref. [1]):

(i) $a(T)<0$ for all $T<T_{cep}$: This means that $l=\infty$ is at least a local maximum of $\Omega_s(l)$. In this case no interfacial wetting transition is possible.

(ii) $a(T)>0$ for all $T<T_{cep}$: This means that $l=\infty$ is always at least a local minimum of $\Omega_s(l)$. If it happens to be its global minimum for all T, the α-γ interface is wet for all T. Otherwise there will be a first-order wetting transition at $T_W<T_{cep}$ depending on higher-order terms in $\omega(l)$.

(iii) $a(T)<0$ for low temperatures and $a(T_{cep})=0^+$: In this case, the interface is not wet at low temperatures, but there is a temperature $T_W<T_{cep}$ with $a(T\geq T_W)\geq0$. For $T\geq T_W$, $l=\infty$ is at least a local minimum. This fulfills the necessary conditions for critical wetting. [The sufficient conditions are determined by higher-order terms of $\omega(l)$ (see Ref. [1]).] In the case of critical wetting $a(T_W)=0$ is an exact, implicit equation for the wetting transition temperature T_W.

(iv) $a(T)>0$ for low temperatures and $a(T_{cep})=0^-$: At

$l=\infty$, $\Omega_s(l)$ has at least a local minimum at low temperatures and a maximum at T_{cep}. In this special case it is possible that an already existing wetting layer undergoes a dewetting transition. An explicit description of the phenomenon is given in Sec. IV of Ref. [38].

In order to determine which binary liquid mixture falls into one of these four classes of interfacial wetting behavior we calculate $a(T)$ for low temperatures and close to T_{cep}. Since $a(T\to T_{cep})/k_BT_{cep}=\kappa\tau^\beta$ vanishes for $T\to T_{cep}$, the necessary condition $a(T_{cep})=0^+$ for interfacial wetting depends only on the sign of κ as long as $\kappa\neq0$. If $\kappa>0$, the α-γ interface is wet at least close to T_{cep}, provided that $l=\infty$ is not only a local but also the global minimum of the effective interface potential. In order to fulfill the necessary conditions for critical wetting $a(T)$ must be negative for low temperatures. Although within the PY theory there is no solid phase, in order to avoid conflicts with a fourth, solid, phase our calculations end at the solidification temperature T_4 without knowing T_4 explicitly [see Figs. 2(a) and 2(b) in Ref. [38]]. The concentration of A particles in the B-rich liquid phase and the concentration of B particles in the A-rich liquid phase decrease with the temperature. For sufficiently low values of T_4 one has

$$\left.\begin{array}{ll}\rho_{A,\alpha}\simeq\rho_A^{(0)} , & \rho_{B,\alpha}\simeq0\\[4pt]\rho_{A,\beta}\simeq0 , & \rho_{B,\beta}\simeq\rho_B^{(0)}\\[4pt]\rho_{A,\gamma}\simeq0 , & \rho_{B,\gamma}\simeq0\end{array}\right\}\text{ at } T_4 \text{ on path } p_1 \qquad (2.17)$$

so that

$$a(T_4)\simeq-\tfrac{1}{2}\rho_B^{(0)}(\rho_B^{(0)}t_{3,BB}-\rho_A^{(0)}t_{3,AB}) , \qquad (2.18)$$

$$\left.\begin{array}{ll}\rho_{A,\alpha}\simeq(0) , & \rho_{B,\alpha}\simeq\rho_B^{(0)}\\[4pt]\rho_{A,\beta}\simeq\rho_A^{(0)} , & \rho_{B,\beta}\simeq0\\[4pt]\rho_{A,\gamma}\simeq0 , & \rho_{B,\gamma}\simeq0\end{array}\right\}\text{ at } T_4 \text{ on path } p_2 \qquad (2.19)$$

so that

$$a(T_4)\simeq-\tfrac{1}{2}\rho_A^{(0)}(\rho_A^{(0)}t_{3,AA}-\rho_B^{(0)}t_{3,AB}) , \qquad (2.20)$$

and

$$\left.\begin{array}{ll}\rho_{A,\alpha}\simeq\rho_A^{(0)} , & \rho_{B,\alpha}\simeq0\\[4pt]\rho_{A,\beta}\simeq0 , & \rho_{B,\beta}\simeq0\\[4pt]\rho_{A,\gamma}\simeq0 , & \rho_{B,\gamma}\simeq\rho_B^{(0)}\end{array}\right\}\text{ at } T_4 \text{ on path } p_3 \qquad (2.21)$$

so that

$$a(T_4) \simeq -\frac{1}{2}\rho_A^{(0)}\rho_B^{(0)}t_{3,AB} \ . \tag{2.22}$$

$\rho_A^{(0)}$ and $\rho_B^{(0)}$ are the densities of the one-component A fluid and the one-component B fluid at their corresponding triple point. On path p_3 the condition $a(T_4) < 0$ is always fulfilled due to the positive sign of $t_{3,AB}$. A first-order wetting transition is not possible along this special path. In order to proceed, for path p_1 and p_2 we make the assumption [38] that

$$\rho_A^{(0)}/\rho_B^{(0)} \simeq (R_B^{(0)}/R_A^{(0)})^3 \ , \tag{2.23}$$

where $R_A^{(0)}$ and $R_B^{(0)}$ are the diameters of the A particles and the B particles, respectively. Thus the condition $a(T_4) < 0$ can be replaced by

$$\bar{t}_{3,BB} > r_0^3 \quad \text{on path } p_1 \ , \tag{2.24}$$

and

$$\bar{t}_{3,AA} > r_0^{-3} \quad \text{on path } p_2 \ , \tag{2.25}$$

with

$$\bar{t}_{3,AA} = \frac{t_{3,AA}}{t_{3,AB}} \ , \quad \bar{t}_{3,BB} = \frac{t_{3,BB}}{t_{3,AB}} \ . \tag{2.26}$$

$r_0 = R_B^{(0)}/R_A^{(0)}$ is the ratio of the diameters of the B particles and the A particles.

According to Weeks, Chandler, and Anderson (see Refs. [43,44] and Appendix B of Ref. [38]) Lennard-Jones interaction potentials $\bar{w}_{ij}(\mathbf{r})$ lead to

$$\bar{w}_{ij}(\mathbf{r}) = \begin{cases} 4\epsilon_{ij}[(\sigma_{ij}/r)^{12} - (\sigma_{ij}/r)^6] \ , & \text{for } r/\sigma_{ij} \geq 2^{1/6} \ , \\ -\epsilon_{ij} \ , & \text{for } r/\sigma_{ij} < 2^{1/6} \ , \end{cases} \tag{2.27}$$

where $\sigma_{AA} \equiv R_A^{(0)}, \sigma_{BB} \equiv R_B^{(0)}$, and $\sigma_{AB} = (\sigma_{AA} + \sigma_{BB})/2$. Following Refs. [38] and [9] one obtains

$$\bar{t}_{3,AA} = \frac{8}{(1+r_0)^3}\bar{w}_{AA} \ , \tag{2.28}$$

$$\bar{t}_{3,BB} = \frac{8r_0^3}{(1+r_0)^3}\bar{w}_{BB} \tag{2.29}$$

with

$$\bar{w}_{AA} = \frac{\hat{w}_{AA}}{\hat{w}_{AB}} \ , \quad \bar{w}_{BB} = \frac{\hat{w}_{BB}}{\hat{w}_{AB}} \ . \tag{2.30}$$

Thus Eqs. (2.9)–(2.30) allow us to classify the interfacial wetting behavior of binary liquid mixtures in terms of the three-dimensional parameter space $\bar{w}_{AA}$, $\bar{w}_{BB}$, and r_0 which determines the bulk number densities and the structure of the bulk phase diagrams.

III. INTERFACIAL WETTING IN THE BLUME-EMERY-GRIFFITHS MODEL

The Blume-Emery-Griffiths model allows one to study binary liquid mixtures with particles of equal size. In this case the reference free-energy density [see Eq. (2.1)] is given by

$$f_h(\rho_i, T) = \sqrt{2}R_A^{-3}k_B T \left\{ \frac{\bar{Q}+\bar{M}}{2}\ln\left[\frac{\bar{Q}+\bar{M}}{2}\right] + \frac{\bar{Q}-\bar{M}}{2}\ln\left[\frac{\bar{Q}-\bar{M}}{2}\right] \right.$$
$$\left. + (1-\bar{Q})\ln(1-\bar{Q}) + \frac{3}{2}\bar{Q}\ln(2^{1/3}R_A^{-2}\Lambda_A\Lambda_B) + \frac{3}{4}\bar{M}\ln\frac{m_B}{m_A} \right\} \tag{3.1}$$

with

$$\bar{Q} = 2^{-1/2}R_A^3(\rho_A + \rho_B) \ , \tag{3.2}$$

$$\bar{M} = 2^{-1/2}R_A^3(\rho_A - \rho_B) \ . \tag{3.3}$$

The effective diameter of the particles $R_A = R_B$ is a function of $R_A^{(0)} = R_B^{(0)}$ [see Eq. (2.27)] and depends only weakly on temperature and density. We disregard this density dependence. m_A and m_B are the masses of the two particles and

$$\Lambda_i = h(2\pi m_i k_B T)^{-1/2} \tag{3.4}$$

is the thermal de Broglie wavelength. Equation (3.1) is the simplest choice of the reference free energy, which reproduces both the low-density limit and the close-packed structure (see Ref. [38]). Combining Eqs. (2.1) and (3.1) gives the following total free-energy density $f = \Omega(\rho_i; T, \mu_i)/V$:

$$f = \sqrt{2}R_A^{-3}\left\{ k_B T\left[\frac{\bar{Q}+\bar{M}}{2}\ln\left[\frac{\bar{Q}+\bar{M}}{2}\right] + \frac{\bar{Q}-\bar{M}}{2}\ln\left[\frac{\bar{Q}-\bar{M}}{2}\right] + (1-\bar{Q})\ln(1-\bar{Q}) \right] \right.$$
$$\left. - \frac{1}{2}(\hat{J}\bar{M}^2 + \hat{K}\bar{Q}^2 + 2\hat{C}\bar{M}\bar{Q}) - H\bar{M} + \Delta\bar{Q} \right\} \tag{3.5}$$

with

$$\hat{J}=\tfrac{1}{4}(\hat{w}_{AA}-2\hat{w}_{AB}+\hat{w}_{BB})\sqrt{2}R_A^{-3}\ , \tag{3.6}$$

$$\hat{K}=\tfrac{1}{4}(\hat{w}_{AA}+2\hat{w}_{AB}+\hat{w}_{BB})\sqrt{2}R_A^{-3}\ , \tag{3.7}$$

$$\hat{C}=\tfrac{1}{4}(\hat{w}_{AA}-\hat{w}_{BB})\sqrt{2}R_A^{-3}\ . \tag{3.8}$$

H and Δ are the field variables conjugate to the unreduced density variables $M=\rho_A-\rho_B$ and $Q=\rho_A+\rho_B$:

$$H=\tfrac{1}{2}(\mu_A-\mu_B)\ , \tag{3.9}$$

$$\Delta=-\tfrac{1}{2}(\mu_A+\mu_B)\ . \tag{3.10}$$

The last two linear terms of Eq. (3.1) are omitted, because they are irrelevant for determining phase equilibria and number densities. Equation (3.5) is the mean-field expression of the free-energy density in the BEG model (see Refs. [45–47]). Using $\hat{J}>0$ as an energy scale, f depends on the dimensionless variables $\hat{T}=k_BT/\hat{J}$, $\hat{H}=H/\hat{J},\overline{\Delta}=\Delta/\hat{J}$, and on the two parameters $\overline{K}=K/\hat{J}$ and $\overline{C}=C/\hat{J}$, which determine the phase diagrams obtained from Eq. (3.1) (see Appendix A). These parameters are given by the interaction potentials

$$\overline{K}=(\overline{w}_{AA}+\overline{w}_{BB}+2)/(\overline{w}_{AA}+\overline{w}_{BB}-2)\ , \tag{3.11}$$

$$\overline{C}=(\overline{w}_{AA}-\overline{w}_{BB})/(\overline{w}_{AA}+\overline{w}_{BB}-2)\ . \tag{3.12}$$

In the following we express $\overline{K}$ and $\overline{C}$ in terms of ζ and Λ as introduced by Scott and Konynenburg (see Refs. [48,35]):

$$\zeta=(\overline{w}_{BB}-\overline{w}_{AA})/(\overline{w}_{AA}+\overline{w}_{BB})\ , \tag{3.13}$$

$$\Lambda=(\overline{w}_{AA}+\overline{w}_{BB}-2)/(\overline{w}_{AA}+\overline{w}_{BB})\ , \tag{3.14}$$

so that

$$\overline{w}_{AA}=(1-\zeta)/(1-\Lambda)\ , \tag{3.15}$$

$$\overline{w}_{BB}=(1+\zeta)/(1-\Lambda)\ . \tag{3.16}$$

This leads to the following relations: $\zeta=-2\overline{C}/(\overline{K}+1)$, $\Lambda=2/(\overline{K}+1),\overline{C}=-\zeta/\Lambda$, and $\overline{K}=-1+2/\Lambda$. Since we are interested in the types of phase diagrams shown in Fig. 1 our analysis is restricted to $\hat{J}>0$ and thus $\Lambda>0$. Due to this restriction and Eqs. (3.13) and (3.14) the (ζ,Λ) parameter space is given by $\zeta\in[-1,1]$ and $\Lambda\in[0,1]$.

In the first step we determine the regions in the parameter space (ζ,Λ) where the corresponding phase diagrams resemble the aforementioned three types of phase diagrams of simple binary liquid mixtures (see Sec. I). For phase diagrams of type II this problem has been solved in Ref. [38]; here we extend this analysis to phase diagrams of the type III. The boundaries of the regions for type-III phase diagrams are obtained numerically. For large values of $|\zeta|$ [i.e., large values of $|\overline{C}|$ in Eq. (3.5)] the concentration of A particles in the B-rich phase and of B particles in the A-rich phase, respectively, and the critical end point temperature T_{cep} decreases to zero (see Sec. II B and Ref. [38]). This leads to numerical problems of small differences between large numbers within the iteration procedure for finding numerical solutions. In order to avoid these problems and a possible solidification of
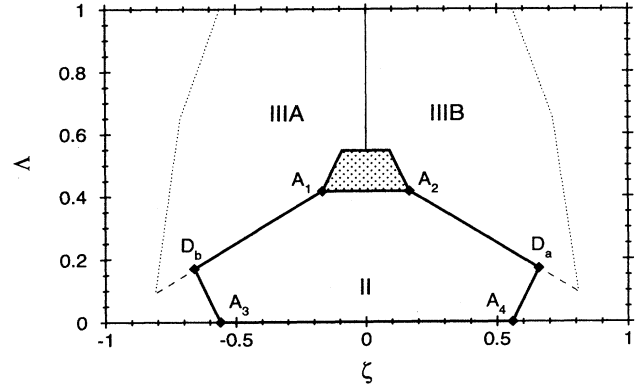
FIG. 4. Boundaries of parameter regions for simple phase diagrams of types II and III within the BEG model. For more details corresponding to type-II phase diagrams see Fig. 2 in Ref. [9]. Here we adopt the same notation as in Refs. [46,9], see Eqs. (3.13) and (3.14). The dotted area is the shield region. The thin dotted lines correspond to the numerical cutoff given by Eq. (3.17). The thin dashed lines are extensions of the lines A_2D_a and A_1D_b, respectively. For those systems lying on the lines A_1D_b and A_2D_a the critical end point T_{cep} happens to be a tricritical point. The same is true for the line separating IIIA and IIIB. Along the lines A_3D_b and A_4D_a tricritical points of a different nature appear (see Ref. [38]).

the system we introduce the following lower cutoff for the concentration of particles:

$$x_{i,\nu}=\left[\frac{\overline{\rho}_i}{\overline{\rho}_A+\overline{\rho}_B}\right]_{\nu,T=T_{\text{cep}}}>1\times10^{-4}\ , \tag{3.17}$$

with $i=A,B$ and $\nu=\alpha,\beta$. We do not consider those systems which violate Eq. (3.17). Figure 4 shows the parameter regions for the different types of simple phase diagrams with the corresponding boundaries. The lines A_1D_b and A_2D_a (see Refs. [9,38]) and the line $(\zeta=0,\Lambda>0)$ correspond to tricritical points (see Sec. I), whereas the line A_3A_4 is given by $\Lambda\to0$ ($\Longrightarrow\overline{K}\to\infty$). The right and left boundaries are due to Eq. (3.17). The dotted area is the so-called shield region (see Refs. [46,49]) containing more complex phase diagrams. In the following we do not discuss this shield region.

In the next step we analyze the wetting behavior at the liquid-vapor interface (see Fig. 3). First we calculate the Hamaker constant $a(T_4)$ at low temperatures (see Sec. II B). Second, we check the condition $a(T_{\text{cep}})=0^+$ (see Appendix C). Figure 5 summarizes our conclusions for the interfacial wetting behavior along the paths p_1 and p_2, whereas Fig. 6 shows the region where interfacial wetting is possible directly in terms of the interactions. In the following we give only a short summary of the main results for the BEG model (the asterisk indicates results at least partly specific for the BEG model), a detailed discussion in comparison with the findings for the more realistic Percus-Yevick theory will follow in Sec. VI.

(1) The interfacial wetting behavior found in Ref. [38] for type-II phase diagrams extends naturally into the region for type-III phase diagrams.
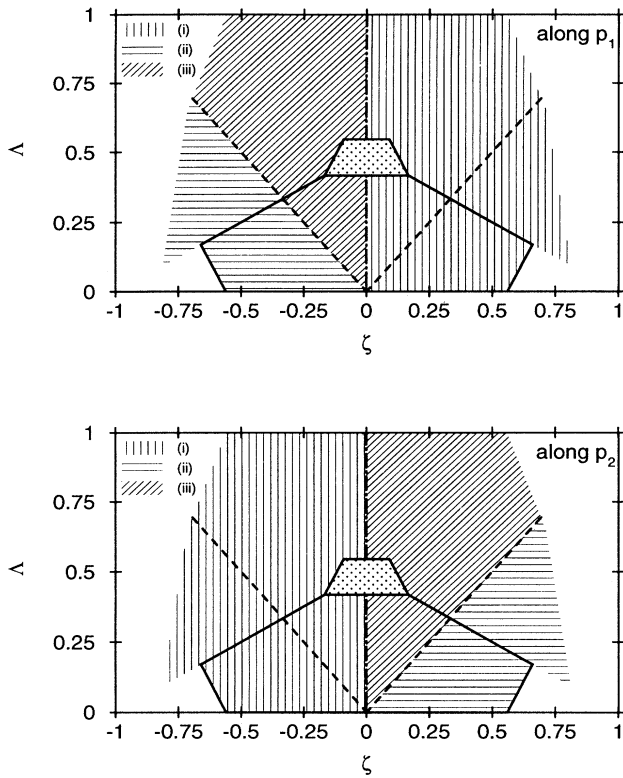
FIG. 5. Classification of binary liquid mixtures with respect to interfacial wetting behavior for the BEG model along the paths p_1 and p_2 within the parameter space defined in Eqs. (3.13) and (3.14). Along path p_3 there is no wetting transition so that this case is not shown. In accordance with Sec. II B, (i) (vertical hatching) corresponds to the absence of interfacial wetting transitions, (ii) (horizontal hatching) corresponds to the occurrence of first-order wetting transitions or that the interface is wet for all temperatures, (iii) (diagonal hatching) represents those systems which can exhibit critical wetting. The dotted area is the shield region. The dash-dotted lines represent those systems with the transition temperature $T_W = T_{cep}$, whereas the dashed lines are related to $T_W = T_4$ where T_4 is the low-temperature limit as described in Sec. II B. The hatching ends due to the cutoff given by Eq. (3.17).

(2*) Within the BEG model interfacial wetting by the vapor phase (along path p_3) is not possible.

(3*) Both for phase diagrams of types II and III the wetting behavior is symmetric about $\zeta = 0$ if the paths p_1 and p_2 are interchanged accordingly.

(4*) The liquid-vapor interface is wetted only by the phase with the lower number density (see Ref. [38]).

(5*) The region in parameter space (ζ, Λ), which allows a first-order wetting transition, is larger than the region with a possibility for critical wetting for type-II phase diagrams. This ratio is reversed for type-III phase diagrams.

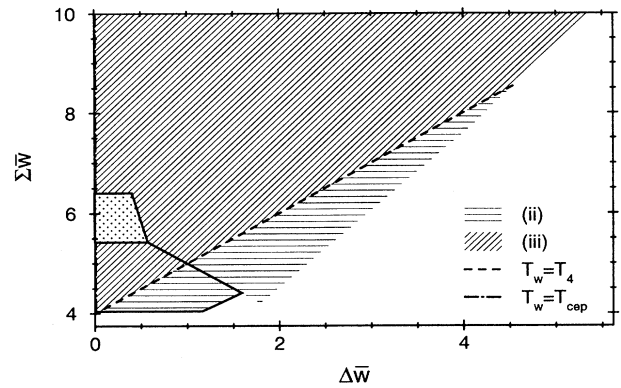(6*) The region in parameter space, which allows for

FIG. 6. Classification of interfacial wetting for the BEG model in terms of $\Sigma\bar{w} = (\hat{w}_{AA} + \hat{w}_{BB} + 2\hat{w}_{AB})/\hat{w}_{AB}$ and $\Delta\bar{w} = (\hat{w}_{AA} - \hat{w}_{BB})/\hat{w}_{AB}$ along path p_1 and $\Delta\bar{w} = (\hat{w}_{BB} - \hat{w}_{AA})/\hat{w}_{AB}$ along path p_2, respectively. We use the same notation as in Fig. 5.

critical wetting, shrinks to zero in the limit that the strengths of the interactions among the two species become equal.

(7*) Both for phase diagrams of types II and III the wetting temperature T_W increases towards T_{cep} if $|\Delta\bar{w}| = |\hat{w}_{AA} - \hat{w}_{BB}|/\hat{w}_{AB}$ goes to zero. In this case the number densities of the pure A and the pure B liquids become similar.

(8*) Within the BEG model dewetting cannot occur.

IV. BULK PROPERTIES OF BINARY LIQUID MIXTURES WITHIN THE PERCUS-YEVICK THEORY

The quantitative predictions of the BEG model are only reliable for small number densities. At larger values of the number densities differences in the particle size become important. In this case a more accurate expression for the reference free-energy density is given by the Percus-Yevick theory with

$$f_h(\rho_i, T) = \sqrt{2} R_A^{-3} k_B T \left[\bar{f}_h(\bar{\rho}_i) + 3 \sum_i \bar{\rho}_i \ln(\Lambda_i / R_A) \right] ,$$

(4.1)

where $\bar{\rho}_i = 2^{-1/2} R_A^3 \rho_i$ and

$$\bar{f}_h(\bar{\rho}_i) = -\bar{p}_h(\bar{\rho}_i) + \sum_i \bar{\rho}_i \bar{\mu}_{h,i}(\bar{\rho}_i) .$$

(4.2)

$\bar{p}_h$ and $\bar{\mu}_{h,i}$ denote the dimensionless pressure and chemical potentials, respectively, of the hard-sphere-fluid mixture, such that

$$p_h(\rho_i, T) = \sqrt{2} R_A^{-3} k_B T \bar{p}_h(\bar{\rho}_i) ,$$

(4.3)

$$\mu_{h,i}(\rho_i, T) = k_B T \bar{\mu}_{h,i}(\bar{\rho}_i) .$$

(4.4)

For $\bar{p}_h$ and $\bar{\mu}_{h,i}$ one finds (see Refs. [50–53])

$$\bar{p}_h(\bar{\rho}_i) = \left[(1 + d_3 + d_3^2) \left[\sum_i \bar{\rho}_i \right] - \frac{\pi}{\sqrt{2}} \bar{\rho}_A \bar{\rho}_B (1 - r)^2 (1 + r + d_2 r) \right] (1 - d_3)^{-3}$$

(4.5)

and

$$\bar{\mu}_{h,i}(\bar{\rho}_i)=\ln[\bar{\rho}_i/(1-d_3)]+3\bar{R}_i d_2/(1-d_3)+\tfrac{9}{2}\bar{R}_i^2 d_2^2/(1-d_3)^2+3\bar{R}_i^2 d_1/(1-d_3)+\frac{\pi}{3\sqrt{2}}\bar{R}_i^3\bar{p}_h(\bar{\rho}_i) \tag{4.6}$$

with $\bar{R}_A=1$, $\bar{R}_B=r=R_B/R_A$, and

$$d_k=\frac{\pi}{3\sqrt{2}}\sum_i \bar{R}_i^k\bar{\rho}_i \ , \quad i=A,B \ , \ k=1,2,3 \ . \tag{4.7}$$

Equations (4.5), (4.6), and (4.7) are approximations of the pressure and of the chemical potential of the reference system, obtained from the Percus-Yevick equation of state for a mixture of hard spheres with diameters R_A and R_B, respectively.

We now proceed in analogy to Sec. III replacing Eq. (3.1) by Eq. (4.1) (see Appendix B for the corresponding changes). The analysis can be restricted to $r \leq 1$ because of the invariance of the free-energy density with respect to an interchange of the particles A and B. The case $r \geq 1$ is given by the following transformations:

$$M \to -M \ , \quad Q \to Q \ , \quad p \to p \ ,$$

$$\mu_A \leftrightarrow \mu_B \ , \quad T \to T \ , \quad H \to -H \ ,$$

$$\Delta \to \Delta \ , \quad \bar{K} \to \bar{K} \ , \quad \bar{C} \to -\bar{C} \ ,$$

$$\bar{t}_{3,AA} \leftrightarrow \bar{t}_{3,BB} \ , \quad \bar{w}_{AA} \leftrightarrow \bar{w}_{BB} \ . \tag{4.8}$$

For not-too-small values of r the PY theory allows one to make quantitative predictions for binary liquid mixtures. [In the extreme case $r \to 0$ the PY equation of state exhibits three deficiencies: (i) In this limit the pair correlation function between the large and small spheres does not fulfill the contact sum rule for the corresponding number density profile of a one-component hard sphere fluid at a hard wall [54], (ii) the distribution function of the large spheres does not reduce to that of a one-component fluid [55], and (iii) the PY equation of state misses the phase separation which has been observed for $r < 0.2$ [56]. However, for $r \geq \tfrac{1}{3}$ the PY equation of state is in good agreement with the data obtained by simulations [57], i.e., the deviations are less than 5%. For $r < \tfrac{1}{3}$ one should use the superposition approximation [54] instead. Since our analysis is confined to $r \geq 0.5$, we therefore can safely use the PY equation of state.] Absolute values of pressure, density, and temperature can be obtained from the reduced quantities by the transformations given in Appendix B. Figure 7 shows experimental data from Streett and Hill [58] for the critical line denoted as L_2 in Fig. 1 for the neon-argon mixture, whereas the corresponding data for neon-xenon in Fig. 8 stem from Deerenberg, Schouten, and Trappeniers [59]. The interaction parameters $\bar{w}_{AA}$, $\bar{w}_{BB}$, and r for the theoretical curves are obtained from Table I of Ref. [38] without trying to find an optimal fit of the experiments. Therefore the comparison between the data and the theoretical curves can be regarded as revealing a qualitatively good agreement for both neon-argon and neon-xenon. Figure 9 shows mass densities of the binary liquid mixture Ar-CH$_4$ obtained from experiments and simulations [60] in comparison with our predictions. Here the interaction

parameters are taken from Table I of Ref. [60]. Our theoretical prediction within the PY theory is in very good agreement both with the experimental data and the data obtained from the molecular-dynamics simulation. Given the fact that the above interaction parameters have not been fitted to the data but taken from independent sources, the predictions appear to be even quantitatively acceptable. The uncertainties in the interaction potential parameters [38] seem to be more relevant than the deficiencies of the PY theory.

The first step in analyzing the parameter space for phase diagrams of type II and type III consists of determining the separatrices between the two types of phase
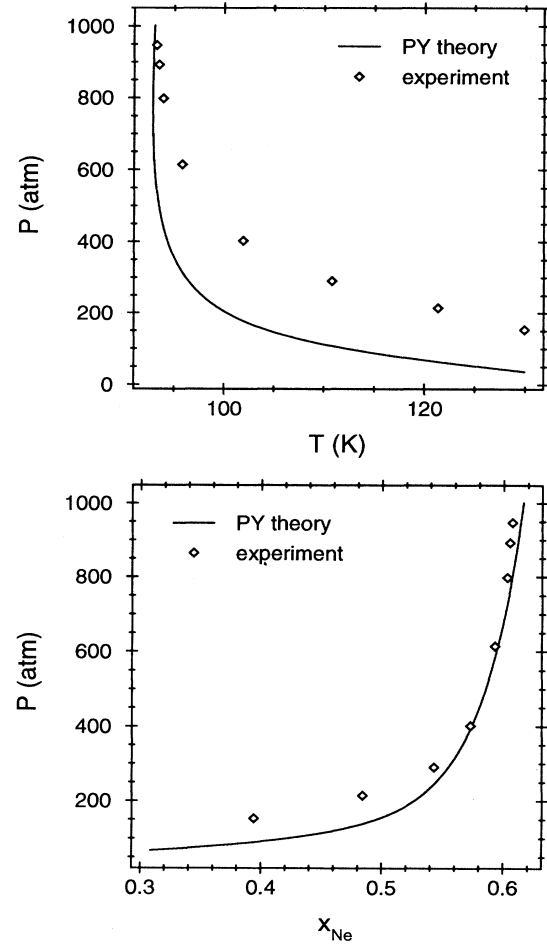

FIG. 7. Experimental data of the critical line L_2 (see Fig. 1) for neon-argon by Streett and Hill [58] in comparison with the predictions of the PY theory. We show the projection of L_2 onto the T-P plane and onto the x_{Ne}-P plane, where x_{Ne} is the neon mole fraction. The Lennard-Jones parameters (see Sec. II B) used for this plot are (particle A denotes argon) $\sigma_{AA}/\text{Å}=3.35$, $\epsilon_{AA}/k_B=143$, $\sigma_{BB}/\text{Å}=2.76$, $\epsilon_{BB}/k_B=42$, $\sigma_{AB}/\text{Å}=3.10$, and $\epsilon_{AB}/k_B=66$.

diagrams. The loci of the tricritical points separating phase diagrams of types II and III have been already determined in Ref. [38]. The third line of tricritical points separating the phase diagrams of types IIIA and IIIB is determined along the lines presented in Appendix A. As mentioned in Sec. III we avoid numerical problems at very low densities by introducing the same cutoff as in Eq. (3.17). In addition, similar problems occur for type-II phase diagrams (see Ref. [38]). In this case the densities in the gas phase are too small. Here, following Ref. [38], we introduce as the cutoff

$$\left[\frac{\bar{\rho}_A}{\bar{\rho}_A + \bar{\rho}_B}\right]_{\text{gas}, T = T_{\text{cep}}} > 5 \times 10^{-3} \qquad (4.9)$$

and

$$(\bar{\rho}_A + \bar{\rho}_B)_{\text{gas}, T = T_{\text{cep}}} > 5 \times 10^{-5} . \qquad (4.10)$$

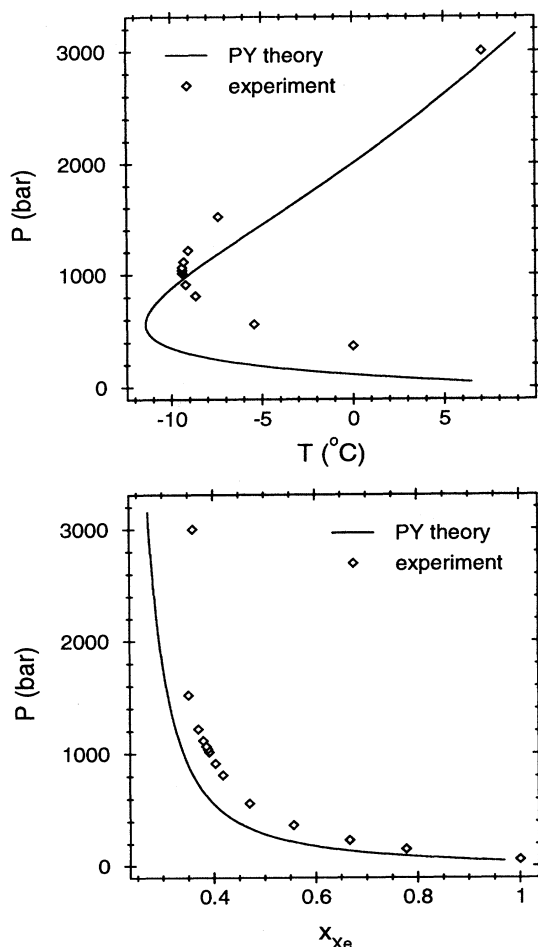Systems which violate Eq. (3.17), (4.9), or (4.10) are dis-

FIG. 8. Experimental data of the critical line L_2 (see Fig. 1) for neon-xenon by Deerenberg, Schouten, and Trappeniers [59] in comparison with the predictions of the PY theory. We show the projection of L_2 onto the T-P plane and onto the x_{Xe}-P plane, where x_{Xe} is the xenon mole fraction. The Lennard-Jones parameters (see Sec. II B) used for this plot are (particle A denotes xenon) $\sigma_{AA}/\text{Å} = 3.92$, $\epsilon_{AA}/k_B = 280$, $\sigma_{BB}/\text{Å} = 2.76$, $\epsilon_{BB}/k_B = 42$, $\sigma_{AB}/\text{Å} = 3.4$, and $\epsilon_{AB}/k_B = 74$.
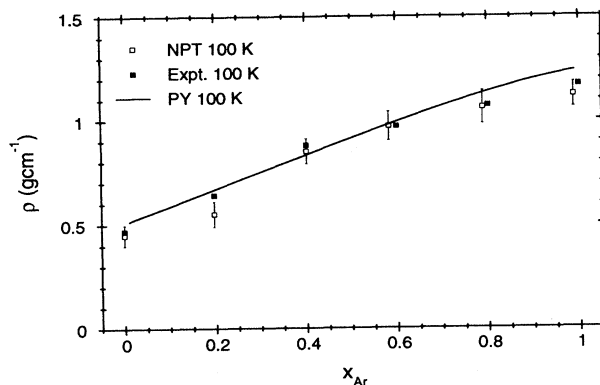

FIG. 9. Mass densities of the Ar-CH$_4$ mixture at 100 K obtained by experiments (black squares) and by [NPT] molecular dynamics with a fixed number of particles, pressure, and temperature (open squares) (see Ref. [60] and references therein) in comparison with the prediction of the PY theory. x_{Ar} is the argon mole fraction. For details see the main text. The Lennard-Jones parameters (see Sec. II B) used for this plot are (particle A denotes CH$_4$) $\sigma_{AA}/\text{Å} = 3.74$, $\epsilon_{AA}/k_B = 152$, $\sigma_{BB}/\text{Å} = 3.40$, $\epsilon_{BB}/k_B = 119.8$, $\sigma_{AB}/\text{Å} = 3.57$, and $\epsilon_{AB}/k_B = 134.9$, whereas the masses are given by $m_A/u = 16.043$ and $m_B/u = 39.95$, where u is the atomic mass unit.

carded. According to our remarks in Sec. I phase diagrams of type IIIA have to fulfill the condition

$$\bar{\rho}_{A,\beta} < \bar{\rho}_{B,\beta} \qquad (4.11)$$

under the assumption that the α phase is B rich and the β phase is A rich, respectively. The shield region has to be calculated numerically for each value of r and is indicated by a dotted triangle. We confine our analysis to $\bar{K} < 100$ which is equivalent to $\Lambda > 0.02$. The results for $r = 1$ are shown in Fig. 10 in comparison with the BEG model.
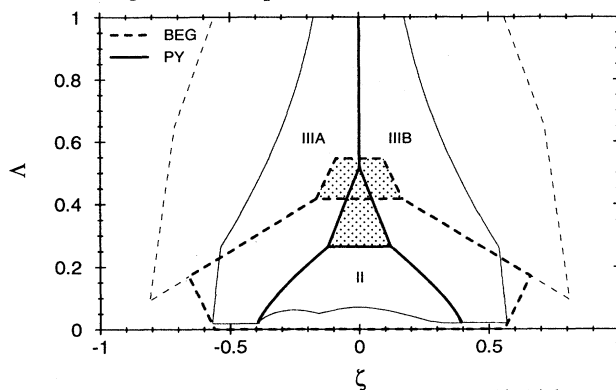

FIG. 10. Separatrices in the parameter space (ζ, Λ) between phase diagrams of type II and type III within the BEG model and the PY theory for $r = 1$. The shield regions are dotted. Within the BEG model the boundaries of the shield region are already known (see Refs. [46,49]); for the PY theory we determine these boundaries numerically by the appearance of more complex phase diagrams. In both cases the actual shape of the shield region is more complicated as shown here. For reasons of simplicity we display only those straight boundaries within which the smaller shield region is embedded. The thin lines correspond to the numerical cutoff described in the main text. The nature of the separatrices is described in Fig. 4 which carries over to the PY theory.
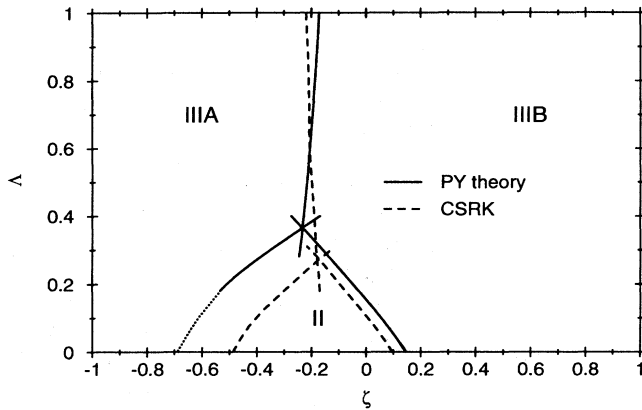
FIG. 11. Tricritical lines (i.e., the loci of those systems which exhibit tricritical points in their phase diagram) in the (ζ, Λ) parameter space as obtained by the PY theory and the Carnahan-Starling-Redlich-Kwong equation of state [61], respectively, for $r = 0.874$. The left tricritical line from the PY theory has been extrapolated (dotted line) due to numerical difficulties mentioned in the main text.

FIG. 12. Tricritical lines (i.e., the loci of those systems which exhibit tricritical points in their phase diagram) in the (ζ, Λ) parameter space as obtained by the PY theory and the Carnahan-Starling-Redlich-Kwong equation of state [61], respectively, for $r = 0.814$. The left tricritical line from the PY theory has been extrapolated (dotted line) due to numerical difficulties mentioned in the main text.

An interesting aspect is a comparison of the lines of tricritical points derived by the PY theory with the same lines obtained by other models. Figures 11 and 12 show our results and those obtained by Kraska and Deiters [61] based on the Carnahan-Starling-Redlich-Kwong (CSRK) equation of state for $r = 0.874$ and $r = 0.814$. The shield regions are omitted. These models turn out to be in fair agreement. The only differences are the shift of the left tricritical line between type-II and -IIIA phase diagrams to larger values of Λ for the PY theory and the different slope of the upper tricritical line. The CSRK equation is a combination of a hard-sphere repulsion term (Carnahan-Starling) and a Redlich-Kwong attraction term [62]. This equation of state is one of the simplest possible noncubic equations, which is justified only heuristically but turns out to be useful for quantitative calculations [61].

V. INTERFACIAL WETTING WITHIN THE PERCUS-YEVICK THEORY

Having mapped out the bulk behavior of binary liquid mixtures we are now in the position to analyze the interfacial wetting behavior in the parameter regions for type-II and type-III phase diagrams. First the behavior at low temperatures is determined by combining Eqs. (2.24), (2.25), (2.28), and (2.29). The condition $a(T_4) < 0$ is given by

$$(1 + \zeta)/(1 - \Lambda) > \tfrac{1}{8}(1 + r)^3 \quad \text{along path } p_1 \qquad (5.1)$$

and

$$(1 - \zeta)/(1 - \Lambda) > \frac{1}{8}\frac{(1 + r)^3}{r^3} \quad \text{along path } p_2 . \qquad (5.2)$$
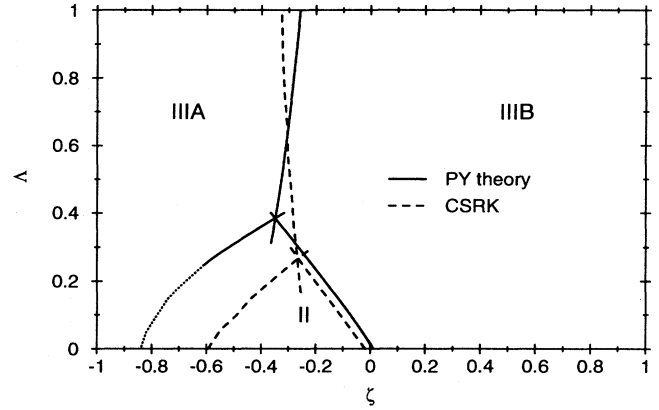
Accordingly a continuous wetting transition can occur at $T_4 < T_W < T_{\text{cep}}$ if either Eq. (5.1) or Eq. (5.2) is fulfilled. Otherwise $l = \infty$ is at least a local minimum of the effective interface potential at low temperatures (see Sec. II B).

In the second step we determine the wetting behavior near T_{cep}. Analogous to the BEG model we calculate the Hamaker constant $a(T)$ (see Appendix C). Close to T_{cep} one has [see Eq. (2.16)]

$$a(T \to T_{\text{cep}}) = k_B T_{\text{cep}} \kappa((T_{\text{cep}} - T)/T_{\text{cep}})^\beta , \qquad (5.3)$$

where β is the standard bulk critical exponent for the order parameter; within MFT $\beta = \tfrac{1}{2}$. According to our previous results the dimensionless amplitude κ is determined uniquely by the parameters ζ, Λ, and r (see Appendix C) which in turn determine the bulk phase diagram. Therefore the location of a specific binary liquid mixture with respect to its bulk properties within this parameter space allows us to analyze its interfacial wetting behavior close to T_{cep} along the paths p_1, p_2, and p_3. Thus we have swept this parameter space and determined κ which yields absolute values for the Hamaker constant close to T_{cep}.

This enables us not only to make predictions for the order of the interfacial wetting transition but it also allows us to determine the thickness l_0 of a complete wetting film close to T_{cep} as long as $a > 0$ (see Refs. [1,40]). In this case we consider thermodynamic paths which lie on the sheet S_2 of α-γ coexistence and approach the triple line TL (see Fig. 1). At constant temperature and for a small distance D off the triple line one has

$$l_0(D \to 0, T) = \left[2^{-3/2} \left[1 + \left[\frac{\partial H_{\alpha\gamma}(\Delta, T)}{\partial \Delta} \bigg|_{\text{TL}} \right]^2 \right]^{-1/2} \left| (Q_\beta - Q_\alpha) - (M_\beta - M_\alpha) \frac{\partial H_{\alpha\gamma}(\Delta, T)}{\partial \Delta} \bigg|_{\text{TL}} \right| \frac{D}{a(T)} \right]^{-1/3} . \qquad (5.4)$$

$H_{\alpha\gamma}(\Delta,T)$ denotes the line of intersection between the sheet S_2 in Fig. 1 and the plane $T=$const, along which we consider complete wetting [see Eqs. (3.9) and (3.10)]. With the exception of D all quantities in Eq. (5.4) are evaluated at the triple line TL for the temperature under consideration.

Experimentally, complete wetting in binary liquid mixtures is easily provided by gravity such that the wetting film of the β phase is floating at a height L above the reservoir of the bulk of the β phase separated by the α phase (see Fig. 4 in Ref. [38]). (This assumes that the wetting phase β has the larger mass density $\bar{\rho}_\beta$ than the wetted phase α.) In this case the height L plays the same role as D in Eq. (5.4). The thickness of such gravity thinned wetting films is given by

$$l_0(L\to0,T)=\left|[\tfrac{1}{4}(m_A+m_B)(Q_\beta-Q_\alpha)\right.$$
$$\left.+\tfrac{1}{4}(m_A-m_B)(M_\beta-M_\alpha)]\frac{gL}{a(T)}\right|^{-1/3} .$$
$$(5.5)$$

Without gravity, i.e., for $g=0$, the system is assumed to be located on the triple line TL.

According to Eqs. (5.4) and (5.5) one has

$$l_0(D\to0,T)=\hat{l}_0(T)D^{-1/3} \qquad (5.6)$$

and

$$l_0(L\to0,T)=\bar{l}_0(T)L^{-1/3} , \qquad (5.7)$$

respectively. Due to Eqs. (2.16), (C1), (5.4), and (5.5) one finds that $\hat{l}_0(T\to T_{cep})$ and $\bar{l}_0(T\to T_{cep})$ remain finite in the case that T_{cep} is an ordinary critical point. This weak temperature dependence of gravity thinned wetting films is in accordance with experimental observations (see Ref. [20]). If, however, T_{cep} happens to be a tricritical point, $a(T\to T_{cep})$ vanishes $\sim\tau^{2\beta^t}$ whereas Q_β-Q_α and M_β-M_α vanish $\sim\tau^{\beta^t}$ for $\tau\to0$ with $\beta^t=\tfrac{1}{2}$ [see Eqs. (C4)–(C7)]. Therefore the thickness of gravity thinned wetting films decreases $\sim\tau^{\beta^t/3}=\tau^{1/6}$ upon approaching a *tricritical point*.

One should emphasize that Eqs. (5.4)–(5.7) are only valid as long as l_0 is large compared with the bulk correlation length ξ [42]. Since $\xi(\tau\to0)=\xi_0\tau^{-\nu}$, $\nu\simeq0.63$, for a critical point and $\xi(\tau\to0)=\xi_0^t\tau^{-\nu^t}$, $\nu^t=1$, for a tricritical point along the triple line, near T_{cep} the validity of Eqs. (5.6) and (5.7) is confined to a near wedgelike region (see Fig. 8 in Ref. [42]):

$$D<\left[\frac{\hat{l}_0}{\xi_0}\right]^3\tau^{3\nu}\sim\tau^{1.89} , \quad L<\left[\frac{\bar{l}_0}{\xi_0}\right]^3\tau^{3\nu}\sim\tau^{1.89}$$

$$\text{(critical point)} \qquad (5.8)$$

and

$$D<\left[\frac{\hat{l}_0}{\xi_0^t}\right]^3\tau^{3\nu^t}\sim\tau^{3\nu^t+\beta^t}=\tau^{3.5} ,$$

$$L<\left[\frac{\bar{l}_0}{\xi_0}\right]^3\tau^{3\nu^t}\sim\tau^{3\nu^t+\beta^t}=\tau^{3.5} .$$

$$\text{(tricritical point)} \qquad (5.9)$$

Outside of this wedgelike region and close to T_{cep} *critical adsorption* occurs which is governed by different growth laws [42]. Equations (5.8) and (5.9) show that a tricritical point confines the wetting growth laws significantly stronger than a critical point.

After we have discussed the importance of the Hamaker constant for complete wetting close to T_{cep} we now return to the amplitude κ which governs its absolute value [see Eq. (5.3)]. Figures 13 and 14 display the dependence of κ on the parameter ζ along typical cuts through the parameter space. Apart from the reduced temperature dependence τ^β, $\tau=(T_{cep}-T)/T_{cep}$, and away from tricritical points and other special points the Hamaker constant is of the order of k_BT_{cep}. Negative values of κ imply that for such binary liquid mixtures close to T_{cep} no macroscopically thick wetting film appears. In turn this is possible for those which correspond to positive values of κ. As displayed in Figs. 13 and 14 this behavior depends on the choice of the thermodynamic path along the triple line. As expected, for a given parameter set κ is positive only for one path and negative for the two other paths. Otherwise Antonov's rule [1] would be violated. Along such cuts through the parameter space one encounters binary liquid mixtures whose critical end point T_{cep} happens to be a tricritical point (see Sec. IV). As discussed in Appendix C for these binary liquid mixtures the Hamaker constant vanishes $\sim\tau^{2\beta^t}$ where β^t is the tricritical exponent for the order parameter along the particular path given by the triple line [36]; within MFT $\beta^t=\tfrac{1}{2}$ which is valid in $d=3$ up to logarithmic correc-
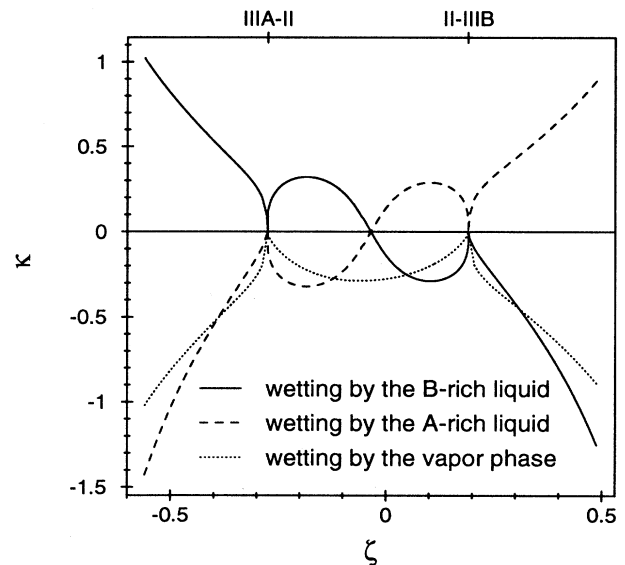

FIG. 13. Dimensionless Hamaker constant κ close to T_{cep} [see Eq. (5.3)] along a certain cut through the parameter space (ζ,Λ,r) which determines the bulk properites of the bindary liquid mixtures. Here we have chosen $\Lambda=0.19$ and $r=0.98$, i.e., the A particles are larger than the B particles. The tricritical points between different types of phase diagrams are indicated by IIIA-II and II-IIIB, respectively. κ vanishes for these values of ζ. The full curve corresponds to path p_1, the dashed curve to path p_2, and the dotted curve to path p_3 (see Sec. II A).
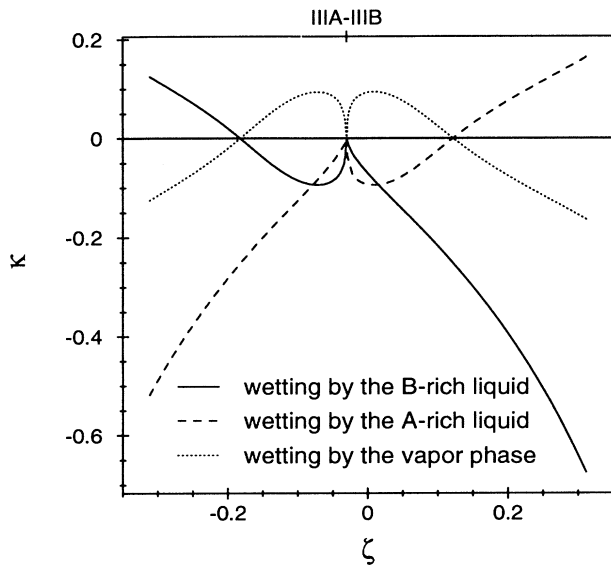
IIIA-IIIB

FIG. 14. Dimensionless Hamaker constant κ close to T_{cep} as in Fig. 13 for $r=0.98$ and $\Lambda=0.61$. The tricritical point between type-IIIA and type-IIIB phase diagrams is indicated by IIIA-IIIB. For all three paths κ vanishes for this value of ζ.

tions. Therefore $a(T \rightarrow T_{cep})/\tau^\beta$ vanishes at a tricritical point. Accordingly κ as defined in Eq. (5.3) vanishes upon approaching a tricritical binary liquid mixture in parameter space. In Fig. 13 this occurs when a type-IIIA phase diagram turns into a type-II phase diagram and when a type-II phase diagram turns into a type-IIIB phase diagram (see Fig. 2); in Fig. 14 type-IIIA and type-IIIB phase diagrams become identical at the tricritical point.

Based on the observation that the Hamaker constant varies monotonously as a function of temperature, it has been argued in Ref. [38] that the remaining zeros of $\kappa(\zeta)$ imply that the corresponding mixtures exhibit a wetting transition temperature, which coincides with T_{cep}. For type-II mixtures this occurs once (see Fig. 13) whereas it occurs twice for type-III mixtures (see Fig. 14).

At this stage it is worthwhile to reconsider Cahn's argument [63,1] which predicts the necessity of a wetting transition upon approaching a critical point, for the case of a tricritical point. According to Cahn close to T_{cep} the contact angle θ varies as $\cos\theta \sim \tau^{\beta_1 - \mu}$ where $\beta_1 \simeq 0.8$ is the critical exponent governing the singular temperature dependence of the order parameter at a free surface and $\mu \simeq 1.26$ describes the variation of the gas-liquid surface tension $\sigma_{gl} \sim \tau^\mu$ with $\tau = (T_{cep} - T)/T_{cep}$. (In fact Cahn [63] did not distinguish between β and the actual exponent β_1). Since $\beta_1 < \mu$, for $\tau \rightarrow 0$ $\cos\theta$ would become larger than 1 signaling the wetting transition. If T_{cep} happens to be a tricritical point, β_1 and μ must be replaced by their tricritical values $\beta_1^t = \frac{3}{2}$ and $\mu^t = 2$ (see Refs. [36,64,65]). We emphasize that these values are appropriate for the particular thermodynamic paths along the triple line corresponding to interfacial wetting. The values quoted above for β_1^t and μ^t are those obtained within MFT. However, in $d=3$ and for tricritical phase

transitions these are the correct values up to logarithmic corrections. Thus we find $\beta_1^t < \mu^t$ as for an ordinary critical point so that Cahn's argument remains valid also for wetting induced by tricritical points.

Figures 13 and 14 display the behavior of the (dimensionless) Hamaker constant for particular cuts through the parameter space. As discussed before the sign of κ together with the low-temperature analysis [see Eqs. (5.1) and (5.2)] allow us to classify the interfacial wetting behavior of binary liquid mixtures. Our corresponding results for a complete sweep of the parameter space (ζ, Λ, r) are documented in Figs. 15–21. (Additional figures are given in Ref. [66].) The allowed region for simple bulk phase diagrams of types II and III is symmetric around $\zeta = 0$ only for $r = 1$. [We consider only those binary liquid mixtures which fulfill the condition $\Lambda > 0.02$ and the inequalities given in Eqs. (3.17), (4.9), (4.10), and (4.11).] The shield region lies within the dotted triangle. The bold lines represent those binary liquid mixtures for
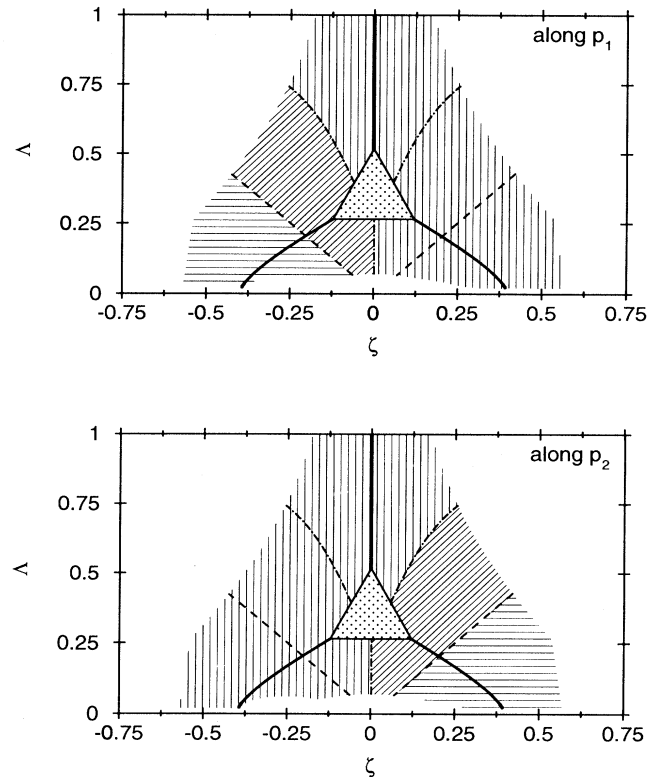

FIG. 15. Interfacial wetting behavior within the PY theory along paths p_1 and p_2 for $r=1.0$. The vertical hatching indicates that an interfacial wetting transition is not possible, a first-order wetting transition or a wet interface for all temperatures is indicated by the horizontal hatching, whereas the diagonal hatching with positive slope represents the possibility for a critical wetting transition. The dotted area includes the shield region. Systems with tricritical points are denoted by bold lines. The dash-dotted lines represent those systems with the wetting transition temperature $T_W = T_{cep}$, whereas the dashed lines are related to systems with $T_W = T_4$ where T_4 is the low-temperature limit as described in Sec. II B. The hatchings end due to certain cutoff values as explained in the main text.
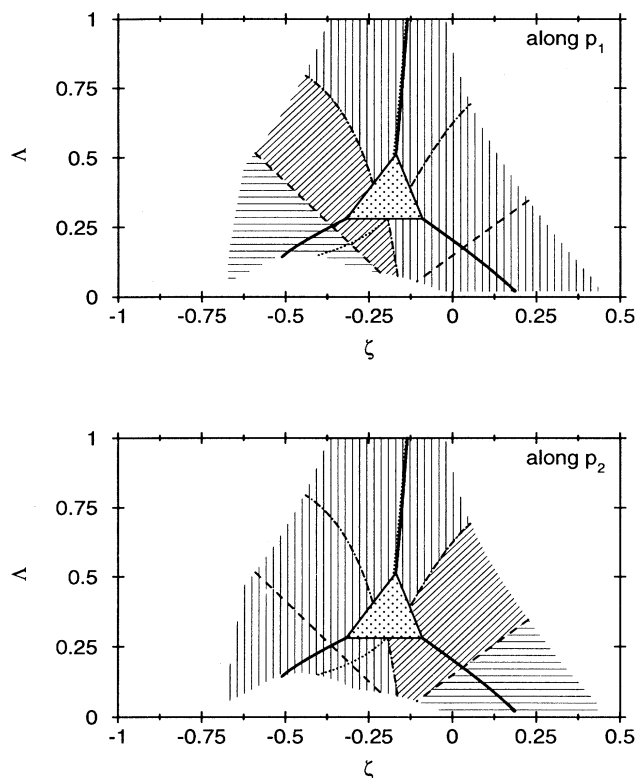
FIG. 16. Interfacial wetting behavior within the PY theory along the paths p_1 and p_2 for $r=0.9$. We use the same notation as in Fig. 15. On the right-hand side of the dotted lines all those binary mixtures lie whose liquid phase being rich in large particles has, at least close to T_{cep}, the lower number density.

FIG. 17. Interfacial wetting behavior as in Fig. 16 for $r=0.82$. Nearly all mixtures of type II lie on the right-hand side of the dotted line.

which T_{cep} happens to be a tricritical point. In accordance with Fig. 10 they divide the parameter space into three regions for phase diagrams of types II, IIIA, and IIIB. The left line of tricritical points disappears for $r<0.7$. The size of the total region for phase diagrams of types II and III decreases for smaller values of r and is shifted to negative values of ζ.

On the right-hand side of the dotted lines (only visible for $0.55 \leq r \leq 0.98$) all those binary liquid mixtures lie whose liquid phase being rich in large particles has, at least close to T_{cep}, the lower number density. The dotted line disappears for $r<0.72$ (type II) and for $r<0.55$ (type IIIA). This means that for small r the liquid phase being rich in small particles always has the higher number density.

The dashed lines are determined by $(1+\zeta)/(1-\Lambda)=\frac{1}{8}(1+r)^3$ and $(1-\zeta)/(1-\Lambda)=\frac{1}{8}(1+r^{-1})^3$, respectively [see Eqs. (5.1) and (5.2)]. These lines determine the behavior of $a(T)$ for low temperatures.

At the dash-dotted lines κ changes sign. As argued in Ref. [38] this means that, in the case of critical wetting, the wetting transition temperature of these binary liquid mixtures coincide with T_{cep}. Thus upon approaching the dash-dotted lines from regions with diagonal hatching with positive slope (see below) the wetting transition tem-
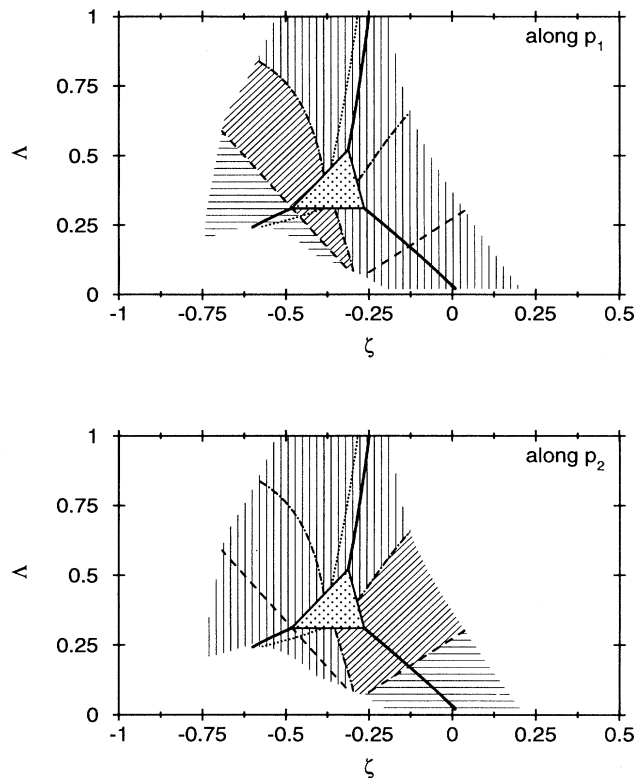
perature approaches T_{cep}. For mixtures with type-II phase diagrams the dash-dotted line coincides with the dotted line for $r=1$.

The classification of the interfacial wetting behavior in the various parameter regions is indicated by different hatchings. The vertical hatching represents the absence of any wetting transition [interfacial wetting behavior of class (i) according to Sec. II B], whereas the horizontal hatching indicates an interfacial wetting transition of first order or a wet interface for all temperatures (ii). The diagonal hatching with positive slope means that the corresponding systems can exhibit critical wetting (iii). The possibility of a dewetting transition (iv) is indicated by a diagonal hatching with negative slope. According to Ref. [38] this behavior is possible only for type-II phase diagrams with $r<0.76$.

In the region for type-II phase diagrams for $r \geq 0.76$ one finds three different kinds of interfacial wetting behavior along the paths p_1 and p_2. For $0.6 \leq r < 0.76$ four classes of interfacial wetting behavior are possible, whereas for $r<0.6$ critical wetting cannot occur along path p_1. For $r \leq 0.5$ also the interfacial wetting behavior of class (i) disappears for path p_1. Extrapolation to smaller values of r indicates, that along both paths p_1 and p_2 only the possibility for first-order interfacial wetting remains. Interfacial wetting by the vapor phase (along path p_3) is not possible for type-II phase diagrams.

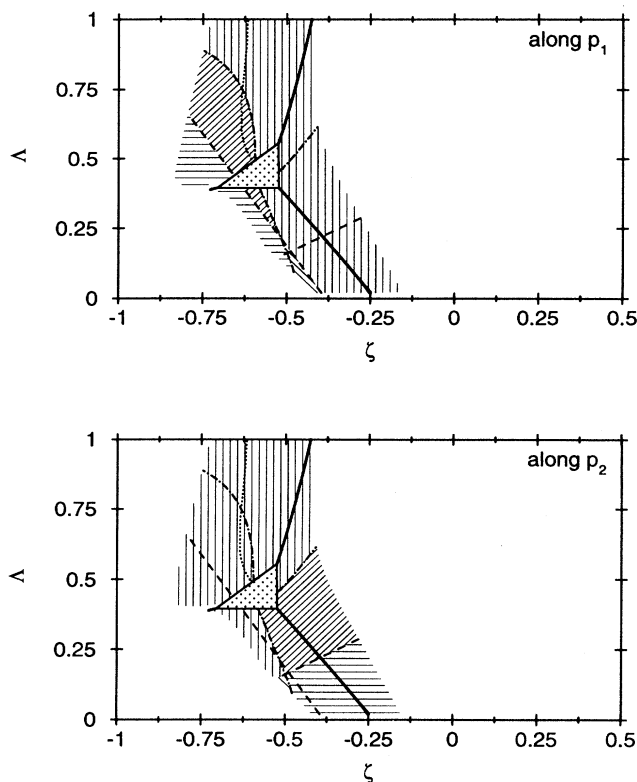Phase diagrams of type III exhibit three classes of in-

FIG. 18. Interfacial wetting behavior as in Figs. 16 and 17 for $r=0.7$. The diagonal hatching with negative slope along p_1 ($\zeta \simeq -0.5$, $\Lambda < 0.25$) indicates the possibility for a dewetting transition (see also the corresponding discussion in Sec. IV of Ref. [38]).
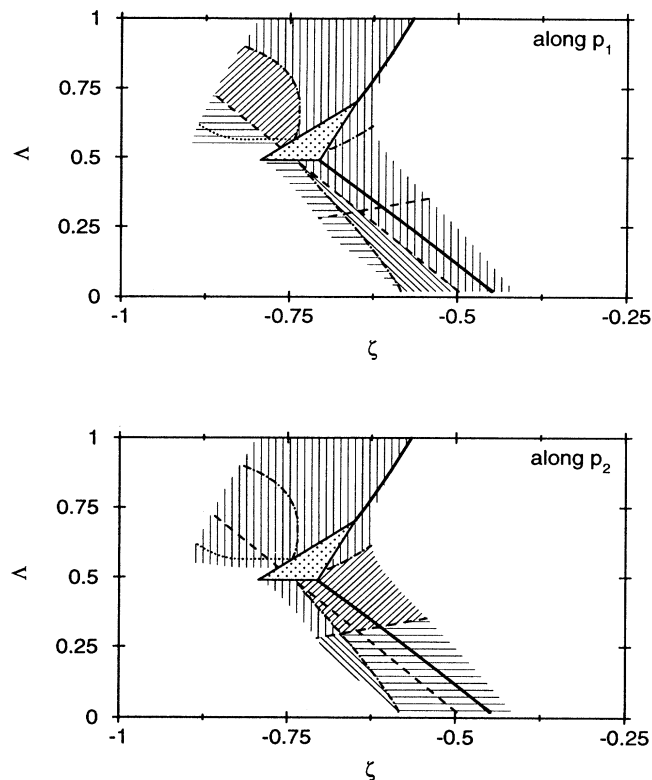
FIG. 19. Interfacial wetting behavior as in Fig. 18 for $r=0.6$. The size of the parameter region, which allows for the occurrence of a dewetting transition, is increased. Dewetting can now take place also along path p_2. Note the expanded scale of the ζ axis.

terfacial wetting behavior along the paths p_1 and p_2 for $r \geq 0.5$. A dewetting transition (iv) does not occur for $r \geq 0.5$ but extrapolation suggests that it may occur for smaller values of r. Contrary to the BEG model and to binary liquid mixtures exhibiting type-II phase diagrams, continuous interfacial wetting by the vapor phase is possible for mixtures with type-III phase diagrams. According to our remarks in Sec. II B first-order wetting (ii) is not possible by the vapor phase.

Besides the very common Lorentz rule for σ_{AB} $=(\sigma_{AA}+\sigma_{BB})/2$, the mixing rule (see Ref. [38])

$$\epsilon_{AB} = \chi (\epsilon_{AA}\epsilon_{BB})^{1/2}, \quad 0 < \chi \leq 1, \tag{5.10}$$

implies the following relationship between ζ and Λ:

$$\Lambda(\zeta) = 1 - \left[\frac{(1+r)^6 \chi^2}{64 r^3}(1-\zeta^2) \right]^{1/2}. \tag{5.11}$$

For $\chi = 1$ Eq. (5.10) is known as the Berthelot rule. The probability for finding binary liquid mixtures within the allowed regions should be enhanced in the vicinity of $\Lambda(\zeta)$ given by Eq. (5.11). In Table I we apply our classification scheme (see Figs. 15–20) for interfacial wetting to a selection of various binary liquid mixtures. The corresponding predictions are based on the Lorentz rule and on the mixing rule with $\chi=0.9$ [see Eq. (5.10)]; this value for χ has proven to be the most adequate choice

[67]. The interaction potentials between similar molecules are taken from Refs. [68,69].

As in Sec. III for the BEG model we summarize our main findings for interfacial wetting predicted by the PY theory.

(1) For the PY theory we have determined the parameter regions where binary liquid mixtures exhibit simple phase diagrams of types II and III.

(2) For $r = 1$ we obtained qualitatively the same results for systems with type-II phase diagrams for both the PY theory and the BEG model. There are only quantitative differences. A qualitative difference is obtained for systems with type-III phase diagrams. For those along the path p_3 critical wetting by the vapor phase is possible. There are mixtures of type II, of type IIIA, and of type IIIB for which in the case of critical wetting the corresponding transition temperature T_W coincides with T_{cep}.

(3) For all values of r critical wetting by the vapor phase is possible for binary liquid mixtures with type-III phase diagrams.

(4) In that region of the parameter space with a possibility of interfacial wetting by the vapor phase no wetting transition by a liquid phase is possible.

(5) Interfacial wetting by a liquid phase occurs only either along path p_1 or along p_2.

(6) In general, the only symmetry is the one which results from the invariance with respect to the interchange
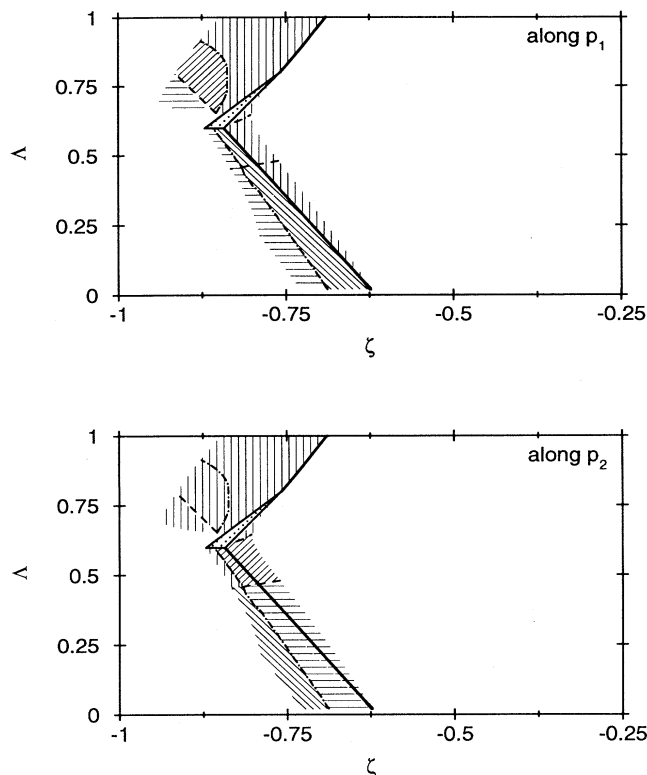
FIG. 20. Interfacial wetting behavior as in Figs. 18 and 19 for $r=0.5$. Note the expanded scale of the ζ axis. The dotted line has disappeared. Thus for $r \leq 0.5$ the liquid phase rich in large particles has, at least close to T_{cep}, the lower number density.

FIG. 21. Interfacial wetting behavior within the PY theory along path p_3 for $r=1.0$ and $r=0.7$. We use the same notation as in Figs. 15 and 18. For mixtures of type III critical wetting by the vapor phase is possible.

of the particles of sort A and B.

(7) For large differences in particle size, i.e., for small r, mixtures of type II exhibit only a possibility for first-order wetting, whereas for mixtures of type III only critical wetting is possible.

(8) Within the parameter region for type-II phase diagrams critical wetting by the liquid phase being rich in small particles cannot occur for $r < 0.6$.

(9) For $r \leq 0.76$ mixtures of type II provide the possibility for a dewetting transition if the wetting layer is rich in the small particles.

VI. SUMMARY

In this section we summarize our main results.

(1) We have studied the bulk properties of binary liquid mixtures within the Percus-Yevick theory (Sec. IV). For certain examples we were able to compare our predictions with those of other theoretical approaches (Figs. 11 and 12), with simulations (Fig. 9), and with experimental data (Figs. 7–9). In general, we find satisfactory agreement.

(2) The scan of the parameter space spanned by the strengths of the interaction potentials and the sizes of the particles allowed us to locate those regions in the parameter space where the binary liquid mixtures exhibit bulk phase diagrams of the types II, IIIA, and IIIB, respec-
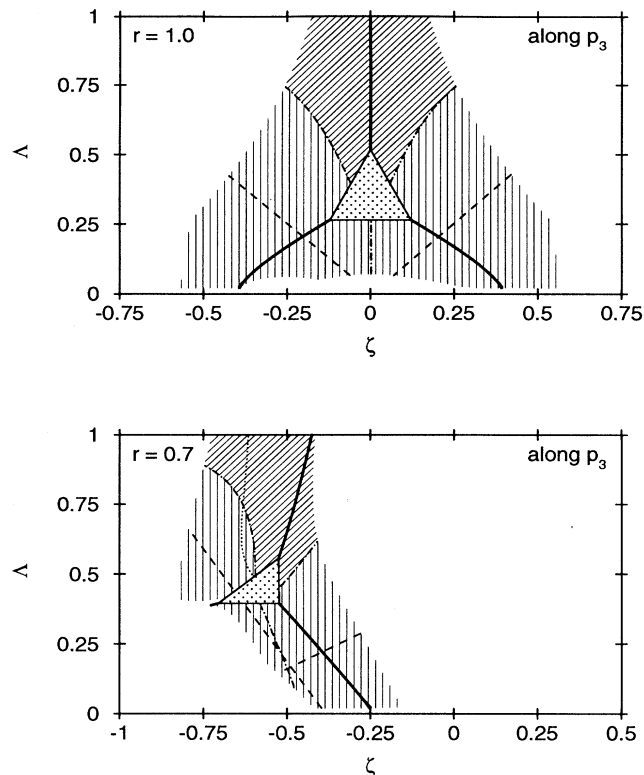
tively, following the nomenclature of Scott and Konynenburg (Fig. 1). Accordingly, we determined those parameters for which binary liquid mixtures happen to have a tricritical point (Fig. 2). These results are presented in Figs. 15–20. The nature of the separatrices between these different regions of the parameter space turns out to be the same as of the corresponding BEG model (see Figs. 4 and 10).

(3) Based on the microscopic expression for the Hamaker constant [Eq. (2.9)] we have classified the interfacial wetting behavior of the binary liquid mixtures described above both within the Blume-Emery-Griffiths model (Sec. III) and for the Percus-Yevick theory (Sec. V). This classification consists of four categories: (i) The α-γ interface (Fig. 3) undergoes no wetting transition, (ii) it either undergoes a first-order wetting transition or it is wet along the whole triple line, (iii) it undergoes critical wetting, and (iv) dewetting occurs. Which category is realized for a given binary liquid mixture depends on whether the wetting phase is the B-rich liquid (path p_1), the A-rich liquid (path p_2), or the vapor phase (path p_3) (Fig. 3). In Figs. 5, 6, and 15–21 this classification is displayed by various hatchings. A detailed summary of these results for the BEG model is given at the end of Sec. III whereas the corresponding summary for the PY theory is presented at the end of Sec. V.

(4) Remarkably for mixtures of type III interfacial wet-

TABLE I. Within the diagonal elements of the table the first and second row give the values for $\sigma_{ii}/\text{Å}$ and ϵ_{ii}/k_B, respectively, as taken from Refs. [68,69]. As discussed in the main text, for $i\neq j$ we choose $\sigma_{ij}=(\sigma_{ii}+\sigma_{jj})/2$ and $\epsilon_{ij}=0.9(\epsilon_{ii}\epsilon_{jj})^{1/2}$. Based on this choice the off-diagonal elements of the table indicate the interfacial wetting behavior of the corresponding binary liquid mixture predicted by Figs. 15–20. The lower-left elements correspond to path p_1 whereas the upper-right elements correspond to path p_2 (see Fig. 1). The symbol ⊠ stands for the absence of an interfacial wetting transition, □ indicates a first-order wetting transition or a wet interface for all temperatures, whereas ◊ denotes the possibility for a critical wetting transition. The symbol △ represents the possibility for a dewetting transition whereas for those cases denoted by ⊗ the critical end point T_{cep} is presumedly preempted by solidification, i.e., $T_4 > T_{\text{cep}}$. [Within our approach this is signaled by violating the inequalities given by Eqs. (4.9) and (4.10).] Binary liquid mixtures which are located outside the hatched regions of Figs. 15–20 are marked by a question mark; the predictions for those systems are inferred by extrapolation. (Note that for the systems discussed in Figs. 7–9 we have chosen slightly different interaction parameters).

	Ammonia	Argon	Methanol	Methane	Xenon	Ethanol	Ethane	1-Butene	Toluene	n-Pentane	n-Hexane	n-Heptane
Ammonia[a]	3.215 309.9	□	□	□	□	◊	□	□	⊗	△	⊗	⊗
Argon[b]	⊠	3.40 122	⊠	⊠	⊠	⊠	⊗	⊗	⊠(?)	⊗	⊠(?)	⊠
Methanol[b]	⊠	□	3.69 234	□	◊	⊠	◊	⊠	⊗(?)	⊠	⊗	⊗
Methane[b]	⊠	□	⊠	3.70 157	⊠	⊠	⊠	⊗	⊠	⊗	⊠(?)	⊠
Xenon[b]	⊠	□	⊠	□	4.06 229	⊠	◊	⊠	⊠(?)	⊠	⊗	⊗
Ethanol[b]	⊠	□	□	□	□	4.34 324	□	◊	⊗	◊	⊗	⊗
Ethane[b]	⊠	⊗	⊠	□	⊠	⊠	4.38 236	⊠	⊠	⊠	⊗	⊗(?)
1-Butene[a]	△	⊗	□	⊗	□	⊠	□	5.274 302.4	⊠	⊠	⊠	⊠
Toluene[b]	⊗	□(?)	⊗(?)	□	□(?)	⊗	□	□	5.64 575	□	◊	◊
n-Pentane[a]	□	⊗	□	⊗	□	⊠	□	◊	⊠	5.916 308.3	⊠	⊠
n-Hexane[b]	⊗	□(?)	⊗	□(?)	⊗	⊗	⊗	□	⊠	□	5.92 517	⊠
n-Heptane[b]	⊗	□	⊗	□	⊗	⊗	⊗(?)	□	⊠	□	◊	6.25 573

[a]Reference [68].
[b]Reference [69].

ting by the vapor phase is possible. For mixtures consisting of particles of rather different sizes dewetting can occur.

(5) We have identified those binary liquid mixtures whose transition temperature for critical wetting coincides with the critical end point T_{cep}.

(6) The above classification scheme is based on the *sign* of the Hamaker constant at low temperature and for $T \rightarrow T_{\text{cep}}$. In addition, we have also determined the *absolute* values of the Hamaker constant close to T_{cep} along cuts through the parameter space (Figs. 13 and 14) and discussed the repercussions for *complete* interfacial wetting close to T_{cep}.

(7) If the critical end point happens to be a tricritical point, Cahn's argument for the necessity of the oc-currence of a wetting transition still applies (Sec. V).

(8) Close to an ordinary critical end point the leading temperature dependence of the thickness of a complete or gravity thinned wetting film drops out. However, if T_{cep} happens to be a tricritical point, the thickness of a complete or gravity thinned wetting film decreases upon approaching T_{cep} (Sec. V).

(9) Specific predictions for the interfacial wetting behavior of various binary liquid mixtures are summarized in Table I.

APPENDIX A: BULK BEG MODEL

Equation (3.5) represents the variational grand canonical free-energy density. Minimization with respect to $\overline{Q}$ and $\overline{M}$ leads to the grand canonical free energy:

$$G(H,\Delta,T)=T\left[\frac{Q+M}{2}\ln\left[\frac{Q+M}{2}\right]+\frac{Q-M}{2}\ln\left[\frac{Q-M}{2}\right]+(1-Q)\ln(1-Q)\right]$$
$$-\tfrac{1}{2}(M^2+KQ^2+2CQM)-HM+\Delta Q \tag{A1}$$

with $G = \min_{\overline{Q}, \overline{M}} (f 2^{-1/2} R_A^3)$. All quantities are reduced and should carry a bar, which is omitted for reasons of clarity. Q and M are functions of H, Δ, and T, and are given implicitly by the simultaneous solutions of (see Refs. [45–47])

$$H = \tfrac{1}{2} T \ln[(Q+M)/(Q-M)] - M - CQ \tag{A2}$$

and

$$\Delta = T \ln[2(1-Q)] - (T/2)\ln(Q^2 - M^2) + CM + KQ \ . \tag{A3}$$

The function

$$Z(M,Q,T) = T \ln(1-Q) + \tfrac{1}{2} M^2 + \tfrac{1}{2} K Q^2 + CMQ \tag{A4}$$

is obtained by inserting Eqs. (A2) and (A3) into Eq. (A1). This leads to

$$G(H, \Delta, T) = Z(M = M(H, \Delta, T), Q = Q(H, \Delta, T), T) \ . \tag{A5}$$

In order to determine critical and tricritical points we perform a Legendre transformation with respect to H [47],

$$\phi(M, \Delta, T) = G(H = H(M, \Delta, T), \Delta, T) + MH(M, \Delta, T) \tag{A6}$$

with

$$\frac{\partial \phi(M, \Delta, T)}{\partial M} = H(M, \Delta, T) \ . \tag{A7}$$

The critical points are determined by the vanishing of the second and third derivative of ϕ with respect to M:

$$\frac{\partial H(M, \Delta, T)}{\partial M} = \frac{\partial^2 H(M, \Delta, T)}{\partial M^2} = 0 \ ,$$
$$\frac{\partial^3 H(M, \Delta, T)}{\partial M^3} > 0 \ . \tag{A8}$$

At a tricritical point in addition the next two higher derivatives of ϕ must vanish:

$$\frac{\partial^n H(M, \Delta, T)}{\partial M^n} = 0 \ , \quad n = 1, \ldots, 4$$
$$\frac{\partial^5 H(M, \Delta, T)}{\partial M^5} > 0 \ . \tag{A9}$$

According to Ref. [38] we have to consider the two functions

$$X(M, Q, T) = \frac{\partial H}{\partial M} - \frac{\partial H}{\partial Q} \frac{\partial \Delta}{\partial M} \left[\frac{\partial \Delta}{\partial Q} \right]^{-1} \tag{A10}$$

with

$$\frac{\partial H(M, \Delta, T)}{\partial M} = X(M, Q = Q(M, \Delta, T), T) \tag{A11}$$

and

$$Y(M, Q, T) = \frac{\partial^2 H}{\partial M^2} - 2 \frac{\partial^2 H}{\partial M \partial Q} \frac{\partial \Delta}{\partial M} \left[\frac{\partial \Delta}{\partial Q} \right]^{-1} - \frac{\partial H}{\partial Q} \frac{\partial^2 \Delta}{\partial M^2} \left[\frac{\partial \Delta}{\partial Q} \right]^{-1} + 2 \frac{\partial H}{\partial Q} \frac{\partial \Delta}{\partial M} \frac{\partial^2 \Delta}{\partial M \partial Q} \left[\frac{\partial \Delta}{\partial Q} \right]^{-2}$$
$$+ \frac{\partial^2 H}{\partial Q^2} \left[\frac{\partial \Delta}{\partial M} \right]^2 \left[\frac{\partial \Delta}{\partial Q} \right]^{-2} - \frac{\partial H}{\partial Q} \frac{\partial^2 \Delta}{\partial Q^2} \left[\frac{\partial \Delta}{\partial M} \right]^2 \left[\frac{\partial \Delta}{\partial Q} \right]^{-3} \tag{A12}$$

with

$$\frac{\partial^2 H(M, \Delta, T)}{\partial M^2} = Y(M, Q = Q(M, \Delta, T), T) \ . \tag{A13}$$

$H \equiv H(M, Q, T)$ and $\Delta \equiv \Delta(M, Q, T)$ are given explicitly by Eqs. (A2) and (A3). The expressions for $\partial^3 H(M, \Delta, T)/\partial M^3$ and $\partial^4 H(M, \Delta, T)/\partial M^4$ are too long in order to present them explicitly.

The critical end point T_{cep} is determined by the following conditions: Eq. (A8) must be fulfilled and H, Δ, as well as the pressure $p = -G(H, \Delta, T)$ must be the same in both the critical phase $\alpha = \beta$ and the coexisting noncritical phase γ. This leads to five coupled nonlinear equations for $M_\alpha = M_\beta$, $Q_\alpha = Q_\beta$, M_γ, Q_γ, and T_{cep}:

$$X(M_\alpha, Q_\alpha, T_{cep}) = 0 \ ,$$
$$Y(M_\alpha, Q_\alpha, T_{cep}) = 0 \ ,$$
$$Z(M_\alpha, Q_\alpha, T_{cep}) = Z(M_\gamma, Q_\gamma, T_{cep}) \ , \tag{A14}$$
$$H(M_\alpha, Q_\alpha, T_{cep}) = H(M_\gamma, Q_\gamma, T_{cep}) \ ,$$
$$\Delta(M_\alpha, Q_\alpha, T_{cep}) = \Delta(M_\gamma, Q_\gamma, T_{cep}) \ .$$

The solutions of Eq. (A14) are determined numerically by iterating suitable initial guesses.

APPENDIX B: BULK PERCUS-YEVICK THEORY

As described in Appendix A all thermodynamic quantities are determined by the functions $H(M, Q, T)$, $\Delta(M, Q, T)$, and $Z(M, Q, T) = -p(M, Q, T)$. Within the Percus-Yevick theory a combination of the Eqs. (2.4), (2.5), (3.2), (3.3), (3.6)–(3.8), and (4.5) leads to

$$Z(M, Q, T) = -T p_h(M, Q) + \tfrac{1}{2} M^2 + \tfrac{1}{2} K Q^2 + CMQ \ , \tag{B1}$$

with

$$p_h(M, Q) = \left[Q(1 + d_3 + d_3^2) - \frac{\pi}{4\sqrt{2}} \gamma_1^2 (Q^2 - M^2)(\alpha_1 + d_2 r) \right] (1 - d_3)^{-3} \tag{B2}$$

where

$$d_k = \frac{\pi}{6\sqrt{2}}(\alpha_k Q + \gamma_k M) \qquad \text{(B3)}$$

and (with $r = R_B/R_A$)

$$\alpha_k = 1 + r^k, \quad \gamma_k = 1 - r^k, \quad k = 1,2,3 . \qquad \text{(B4)}$$

All quantities are reduced and should carry a bar. For reasons of clarity we omit these bars. Nonreduced quantities can be obtained by the following transformations:
$-Z = p \rightarrow 2^{-1/2}R_A^3 p/\hat{J}, \qquad T \rightarrow k_B T/\hat{J}, \qquad K \rightarrow K/\hat{J},$
$C \rightarrow C/\hat{J}, \quad M \rightarrow 2^{-1/2}R_A^3 M, \quad Q \rightarrow 2^{-1/2}R_A^3 Q, \quad H \rightarrow H/\hat{J},$
$\Delta \rightarrow \Delta/\hat{J}$, where

$$H = T\left\{\tfrac{1}{2}\ln\left[\frac{Q+M}{Q-M}\right] - 3\frac{\gamma_1\gamma_2}{\gamma_3} + 3\left[\frac{\gamma_1\gamma_2}{\gamma_3} + \frac{\pi}{6\sqrt{2}}Q\left[\gamma_3 - \alpha_3\frac{\gamma_1\gamma_2}{\gamma_3}\right]\right](1-d_3)^{-1}\right.$$
$$\left. + \tfrac{9}{4}\gamma_2 d_2^2(1-d_3)^{-2} + \frac{\pi}{6\sqrt{2}}\gamma_3 p_h(M,Q)\right\} - M - CQ \qquad \text{(B5)}$$

and

$$\Delta = T\left[-\tfrac{1}{2}\ln(Q^2 - M^2) + \ln(1-d_3) - 3\left[1 + \frac{\pi}{6\sqrt{2}}Q(\alpha_1\alpha_2 - \alpha_3)\right](1-d_3)^{-1}\right.$$
$$\left. + 3 - \tfrac{9}{4}\alpha_2 d_2^2(1-d_3)^{-2} - \frac{\pi}{6\sqrt{2}}\alpha_3 p_h(M,Q)\right] + CM + KQ . \qquad \text{(B6)}$$

Note the relation $\alpha_1\gamma_2 + \alpha_2\gamma_1 = 2\gamma_3$.

In general, the ratio of diameters $r = R_B/R_A$ depends on r_0, $k_B T/\hat{J}$, $\hat{K}/\hat{J}$, whereas at T_{cep} it depends on r_0, $\hat{K}/\hat{J}$, and $\hat{C}/\hat{J}$. Both R_A and R_B are increasing functions of the temperature, but the ratio r exhibits a weaker dependence. Therefore we approximate r by the constant r_0, which eases our numerical scan through the parameter space ζ and Λ.

All of the formulas used in this paper are based on the compressibility relation (see Refs. [52,53]):

$$1 - \sum_i \rho_i c_{ij}^{(2)}(\mathbf{q}=0) = \frac{\partial p_h}{\partial \rho_j}\bigg/(k_B T) ,$$
$$\rho_i c_{ij}^{(2)}(\mathbf{q}=0) = \delta_{ij} - \rho_i\frac{\partial \mu_{h,i}}{\partial \rho_j}\bigg/(k_B T) , \qquad \text{(B7)}$$

where $c_{ij}^{(2)}(\mathbf{q})$ is the Fourier transform of the direct correlation function $c_{ij}^{(2)}(\mathbf{r}_1 - \mathbf{r}_2)$ (see Appendix A in Ref. [38]). According to Eq. (4.2) the reference free energy is given by p_h and $\mu_{h,i}$. By using Eq. (B7) one can obtain the following relations between Z, H, and Δ:

$$\frac{\partial Z}{\partial Q} = Q\frac{\partial \Delta}{\partial Q} - M\frac{\partial H}{\partial Q} ,$$
$$\frac{\partial Z}{\partial M} = Q\frac{\partial \Delta}{\partial M} - M\frac{\partial H}{\partial M} . \qquad \text{(B8)}$$

Equation (B8) provides a useful test for the correctness of the numerical calculations.

APPENDIX C: HAMAKER CONSTANT

In the limit $T \rightarrow T_{cep}$ both differences $M_\alpha - M_\beta$ and $Q_\alpha - Q_\beta$ [see Eqs. (2.10) and (2.11)] vanish as a power law with the critical exponent β:

$$M_\alpha - M_\beta \simeq \kappa_{M_{\alpha,\beta}}\tau^\beta , \quad Q_\alpha - Q_\beta \simeq \kappa_{Q_{\alpha,\beta}}\tau^\beta . \qquad \text{(C1)}$$

where $\tau = (T_{cep} - T)/T_{cep}$ and within mean-field theory

$$\beta = \tfrac{1}{2} . \qquad \text{(C2)}$$

The amplitude κ as defined in Eq. (2.16) is given by

$$\kappa = [(\kappa_{M_{\alpha,\beta}} + \kappa_{Q_{\alpha,\beta}})\{(M_\beta - M_\gamma) + (Q_\beta - Q_\gamma)\}\bar{t}_{3,AA} + (\kappa_{M_{\alpha,\beta}} - \kappa_{Q_{\alpha,\beta}})\{(M_\beta - M_\gamma) - (Q_\beta - Q_\gamma)\}\bar{t}_{3,BB}$$
$$+ 2\{\kappa_{Q_{\alpha,\beta}}(Q_\beta - Q_\gamma) - \kappa_{M_{\alpha,\beta}}(M_\beta - M_\gamma)\}]\frac{t_{3,AB}}{8k_B T_{cep}} . \qquad \text{(C3)}$$

In Eq. (2.16) M_β, M_γ, Q_β, and Q_γ are evaluated at $T = T_{cep}$. At a tricritical point T_{tric} all three phases become critical and identical. Therefore the following four differences of the density variables M and Q vanish for $T \rightarrow T_{tric}$:

$$M_\alpha - M_\beta \sim \kappa_{M_{\alpha,\beta}}\tau^{\beta^t} , \quad Q_\alpha - Q_\beta \sim \kappa_{Q_{\alpha,\beta}}\tau^{\beta^t} , \qquad \text{(C4)}$$

$$M_\beta - M_\gamma \sim \kappa_{M_{\beta,\gamma}}\tau^{\beta^t} , \quad Q_\beta - Q_\gamma \sim \kappa_{Q_{\beta,\gamma}}\tau^{\beta^t} . \qquad \text{(C5)}$$

Along the special path given by the triple line the tricritical exponent β^t is given by (see Ref. [36])

$$\beta^t = \tfrac{1}{2} . \qquad \text{(C6)}$$

In $d=3$ Eq. (C6) is valid beyond MFT up to logarithmic corrections. As a consequence of $T \to T_{\text{cep}} = T_{\text{tric}}$, $a(T)$ vanishes as $\tau^{2\beta^t}$,

$$\frac{a(T)}{k_B T_{\text{tric}}} = \kappa' \tau^{2\beta^t}, \quad \text{for } T \to T_{\text{cep}} = T_{\text{tric}}, \tag{C7}$$

with

$$\kappa' = [(\kappa_{M_{\alpha,\beta}} + \kappa_{Q_{\alpha,\beta}})(\kappa_{M_{\beta,\gamma}} + \kappa_{Q_{\beta,\gamma}})\bar{t}_{3,AA} + (\kappa_{M_{\alpha,\beta}} - \kappa_{Q_{\alpha,\beta}})(\kappa_{M_{\beta,\gamma}} - \kappa_{Q_{\beta,\gamma}})\bar{t}_{3,BB} + 2(\kappa_{Q_{\alpha,\beta}}\kappa_{Q_{\beta,\gamma}} - \kappa_{M_{\alpha,\beta}}\kappa_{M_{\beta,\gamma}})] \frac{t_{3,AB}}{8k_B T_{\text{tric}}}. \tag{C8}$$

Since $2\beta^t > \beta$ the amplitude κ [see Eq. (C3)] vanishes for those binary liquid mixtures whose critical end point happens to be a tricritical point.

For the classification of wetting behavior it is sufficient to calculate only the sign of $a(T)$. In this case we use the following form of Eq. (2.9):

$$a(T) = \tfrac{1}{8}(Q_\alpha - Q_\beta)(Q_\beta - Q_\gamma)[(1 + \tilde{\lambda}_{\alpha\beta})(1 + \tilde{\lambda}_{\beta\gamma})\bar{t}_{3,AA} + (1 - \tilde{\lambda}_{\alpha\beta})(1 - \tilde{\lambda}_{\beta\gamma})\bar{t}_{3,BB} + 2(1 - \tilde{\lambda}_{\alpha\beta}\tilde{\lambda}_{\beta\gamma})]t_{3,AB} \tag{C9}$$

with

$$\tilde{\lambda}_{\alpha\beta} = (M_\alpha - M_\beta)/(Q_\alpha - Q_\beta) \tag{C10}$$

and

$$\tilde{\lambda}_{\beta\gamma} = (M_\beta - M_\gamma)/(Q_\beta - Q_\gamma). \tag{C11}$$

At the critical end point T_{cep}, $\lambda_{\alpha\beta} = \tilde{\lambda}_{\alpha\beta}(T = T_{\text{cep}})$ is given by

$$\lambda_{\alpha\beta} = \kappa_{M_{\alpha,\beta}}/\kappa_{Q_{\alpha,\beta}}. \tag{C12}$$

Within a straightforward approach one would determine $\lambda_{\alpha\beta}$ by taking the limit $\tilde{\lambda}_{\alpha\beta}(\tau \to 0)$ along the triple line for

each value of ζ and Λ. However, the numerical efforts can be reduced substantially by expanding $H(M,Q,T)$ [see Eq. (A2)] around $(M_{\text{cep}}, Q_{\text{cep}}, T_{\text{cep}})$ (see Ref. [38]) which leads to

$$\lambda_{\alpha\beta} = -\frac{\partial H(M,Q,T)}{\partial Q}\bigg|_{M_C, Q_C, T_C}$$
$$\times \left[\frac{\partial H(M,Q,T)}{\partial M}\bigg|_{M_C, Q_C, T_C}\right]^{-1}, \tag{C13}$$

which can be evaluated directly without performing the limit $\tau \to 0$ numerically.

[1] S. Dietrich, in *Phase Transitions and Critical Phenomena*, edited by C. Domb and J. L. Lebowitz (Academic, London, 1988), Vol. 12, p. 1.

[2] J. S. Rowlinson and B. Widom, *Molecular Theory of Capillarity* (Clarendon, Oxford, 1982).

[3] R. Pandit, M. Schick, and M. Wortis, Phys. Rev. B **26**, 5112 (1982).

[4] E. H. Hauge, in *Fundamental Problems in Statistical Mechanics VI*, edited by E. G. D. Cohen (North-Holland, Amsterdam, 1985), p. 65.

[5] M. Wortis, in *Fundamental Problems in Statistical Mechanics VI*, [4], p. 87.

[6] G. P. de Gennes, Rev. Mod. Phys. **57**, 827 (1985).

[7] D. E. Sullivan and M. M. Telo da Gama, in *Fluid Interfacial Phenomena*, edited by C. A. Croxton (Wiley, New York, 1986), p. 45.

[8] M. Schick, in *Liquids at Interfaces*, Proceedings of the Les Houches Summer School, edited by J. Charvolin, J. F. Joanny, and J. Zinn-Justin (North-Holland, Amsterdam, 1989), p. 415.

[9] S. Dietrich and M. Schick, Phys. Rev. B **33**, 4952 (1986).

[10] D. W. Pohl and W. I. Goldburg, Phys. Rev. Lett. **48**, 185 (1982).

[11] D. Beysens and D. Estéve, Phys. Rev. Lett. **54**, 2123 (1985).

[12] L. Sigl and W. Fenzl, Phys. Rev. Lett. **57**, 2191 (1986).

[13] X. Wu, M. Schlossman, and C. Franck, Phys. Rev. B **33**,

402 (1986).

[14] K. Abeysuriya, X. Wu, and C. Franck, Phys. Rev. B **35**, 6771 (1987).

[15] D. J. Durian and C. Franck, Phys. Rev. Lett. **59**, 555 (1987).

[16] D. J. Durian and C. Franck, Phys. Rev. B **36**, 7307 (1987).

[17] S. Dietrich, M. P. Nightingale, and M. Schick, Phys. Rev. B **32**, 3182 (1985).

[18] R. B. Heady and J. W. Cahn, J. Chem. Phys. **58**, 896 (1973).

[19] M. R. Moldover and J. W. Cahn, Science **207**, 1073 (1980).

[20] O'D. Kwon, D. Beaglehole, W. W. Webb, B. Widom, J. W. Schmidt, J. W. Cahn, M. R. Moldover, and B. Stephenson, Phys. Rev. Lett. **48**, 185 (1982).

[21] D. Beaglehole, J. Phys. Chem. **87**, 4749 (1983).

[22] J. W. Schmidt and M. R. Moldover, J. Phys. Chem. **79**, 379 (1983).

[23] V. Vani, S. Guha, E. S. R. Gopal, and S. M. Rao, Phys. Lett. **99A**, 441 (1983).

[24] M. R. Moldover and J. W. Schmidt, Physica D **12**, 351 (1984).

[25] C. Houessou, P. Guenoun, R. Gastaud, F. Perrot, and D. Beysens, Phys. Rev. A **32**, 1818 (1985).

[26] S. Chatterjee, V. Vani, S. Guha, and E. S. R. Gopal, J. Phys. (Paris) **46**, 1533 (1985).

[27] J. W. Schmidt and M. R. Moldover, J. Chem. Phys. **84**,

4563 (1986).

[28] J. Gracia, C. Guerrero, J. G. Llanes, and A. Robledo, J. Phys. Chem. **90**, 1350 (1986).

[29] F. Guzman and J. W. Schmidt, J. Phys. Chem. **91**, 263 (1987).

[30] J. W. Schmidt, J. Colloid Interface Sci. **122**, 575 (1988).

[31] M. Kahlweit, G. Busse, D. Haase, and J. Jen, Phys. Rev. A **38**, 1395 (1988).

[32] P. Tarazona, M. M. Telo da Gama, and R. Evans, Mol. Phys. **49**, 283 (1983).

[33] P. Tarazona, M. M. Telo da Gama, and R. Evans, Mol. Phys. **49**, 301 (1983).

[34] P. Tarazona, R. Evans, and U. M. B. Marconi, Mol. Phys. **54**, 1357 (1985).

[35] R. L. Scott and P. H. van Konynenburg, Discuss. Faraday Soc. **49**, 87 (1970).

[36] I. D. Lawrie and S. Sarbach, in *Phase Transitions and Critical Phenomena,* edited by C. Domb and J. L. Lebowitz (Academic, London, 1984), Vol. 9, p. 1.

[37] B. Widom, in *Liquids, Freezing and Glass Transition,* 1989, Les Houches Lectures, edited by J. P. Hansen, D. Levesque, and J. Zinn-Justin (Elsevier, Amsterdam, 1991), Course 6, p. 505.

[38] S. Dietrich and A. Latz, Phys. Rev. B **40**, 9204 (1989).

[39] J. N. Israelachvili, *Intermolecular and Surface Forces* (Academic, London, 1985).

[40] M. Napiórkowski and S. Dietrich, Phys. Rev. B **34**, 6469 (1986).

[41] S. Dietrich and M. Napiórkowski, Phys. Rev. A **43**, 1861 (1991).

[42] S. Dietrich, in *Phase Transitions in Surface Films 2,* Vol. 267 of NATO Advanced Study Institute, Series B: *Physics,* edited by H. Taub, G. Torzo, H. J. Lauter, and S. C. Fain (Plenum, New York, 1991), p. 391.

[43] J. D. Weeks, D. Chandler, and H. C. Anderson, J. Chem. Phys. **54**, 5237 (1971).

[44] H. C. Anderson, J. D. Weeks, and D. Chandler, Phys. Rev. A **4**, 1597 (1971).

[45] M. Blume, V. Emery, and R. B. Griffiths, Phys. Rev. A **4**, 1071 (1971).

[46] D. Furman, S. Dattagupta, and R. B. Griffiths, Phys. Rev. B **15**, 441 (1977).

[47] D. Mukamel and M. Blume, Phys. Rev. A **10**, 610 (1974).

[48] P. H. van Konynenburg and R. L. Scott, Philos. Trans. R. Soc. London, Ser. A **298**, 495 (1980).

[49] D. Furman and R. B. Griffiths, Phys. Rev. A **17**, 1139 (1978).

[50] H. L. Frisch and J. L. Lebowitz, *The Equilibrium Theory of Classical Fluids* (Benjamin, New York, 1964), p. II-300.

[51] J. L. Lebowitz, E. Helfand, and E. Praestgaard, J. Chem. Phys. **43**, 774 (1965).

[52] J. L. Lebowitz and E. M. Waisman, in *The Liquid State of Matter: Fluids, Simple and Complex,* edited by E. W. Montroll and J. L. Lebowitz (North-Holland, Amsterdam, 1982), p. 1.

[53] J. L. Lebowitz, Phys. Rev. **133**, A895 (1964).

[54] J. Fischer, Mol. Phys. **33**, 75 (1977).

[55] T. Biben and J.-P. Hansen, Europhys. Lett. **12**, 347 (1990).

[56] T. Biben and J.-P. Hansen, Phys. Rev. Lett. **66**, 2215 (1991).

[57] J. L. Lebowitz and J. S. Rowlinson, J. Chem. Phys. **41**, 133 (1964).

[58] W. B. Streett and J. L. E. Hill, J. Chem. Phys. **54**, 5088 (1971).

[59] A. Deerenberg, J. A. Schouten, and N. J. Trappeniers, Physica A **101**, 459 (1980).

[60] D. M. Heyes, J. Chem. Phys. **96**, 2217 (1992).

[61] T. Kraska and U. K. Deiters, J. Chem. Phys. **96**, 539 (1992).

[62] U. K. Deiters and I. L. Pegg, J. Chem. Phys. **90**, 6632 (1989).

[63] J. W. Cahn, J. Chem. Phys. **66**, 3667 (1977).

[64] K. Binder, in *Phase Transitions and Critical Phenomena,* edited by C. Domb and J. L. Lebowitz (Academic, London, 1983), Vol. 8, p. 1.

[65] H. W. Diehl and E. Eisenriegler, Europhys. Lett. **4**, 709 (1987); E. Eisenriegler and H. W. Diehl, Phys. Rev. B **37**, 5257 (1988).

[66] T. Getta, diploma thesis, WUD 91-17, University of Wuppertal, 1991.

[67] G. C. Maitland, M. Rigby, E. B. Smith, and W. A. Wakeham, *Intermolecular Forces* (Clarendon, Oxford, 1981).

[68] F. M. Mourits and F. H. A. Rummens, Can. J. Chem. **55**, 3007 (1977).

[69] E. Wilhelm and R. Battino, J. Chem. Phys. **55**, 4012 (1971).